Technische Universität München
Fakultät für Physik

Quantum Science and Technology Master's thesis

Quantum tensor networks for sampling

Simon Botond

13. September 2025

Erstgutachter (Themensteller): Dr. Jeanette Miriam-Lorentz
Zweitgutachter: Alex Goessmann

Abstract

Efficient sampling from complex probability distributions is a cornerstone of modern Artificial Intelligence workflows, enabling critical tasks such as probabilistic inference, generative modeling, and optimization. Classical sampling methods, including brute force or Markov Chain Monte Carlo methods, face prohibitive computational challenges as the dimensionality and logical complexity of target distributions grow. This thesis investigates the potential of quantum computing - specifically amplitude amplification algorithms - to overcome these limitations and deliver practical advantages for machine learning sampling tasks. Through a systematic methodology, logical connectives and graphical models are mapped to quantum circuits via the Tensor network decomposition of their exponential family distributions. Simulations on up to ≈ 25 qubits (variables and ancillas together) demonstrate the scalability of quantum amplitude amplification, while comparative analyses with classical baselines quantify speedup and a possible turnover point. The results reveal that quantum-assisted sampling achieves quadratic speedups for structured distributions, though hardware constraints and noise pose significant challenges. This work bridges quantum computing and machine learning by formalizing a framework for integrating quantum sampling into classical workflows, offering a pathway toward scalable probabilistic inference in AI systems.

Contents

Chapter 1

Introduction

Motivation and Background

Sampling is an essential part of a machine learning algorithm. Whenever the program makes a decision, handles predictions with uncertainty or gives solutions to a problem, it is a form of sampling from a vast set of information. This set is usually called data or knowledge. Sampling therefore is fundamental in enabling probabilistic inference, uncertainty quantification, and optimization in high-dimensional spaces. As models are increasingly sophisticated - incorporating rich logical structures or large graphical dependencies - their complexity escalates and the computational demands of sampling algorithms grow exponentially. Classical methods, while foundational, struggle to balance accuracy and efficiency in high-dimensional or multimodal distributions. Quantum computing, with its inherent parallelism and interference capabilities suggest that quantum algorithms could offer speedups for certain sampling tasks. This motivates a systematic investigation of their applicability and impact for artificial intelligence [1][2]. This thesis explores the intersection of quantum computing and AI, focusing on how quantum amplitude amplification can revolutionize sampling tasks in artificial intelligence. The following sections elaborate on the background and motivation, objectives, challenges, and the structure of this work.

Machine Learning and Artificial Intelligence

Machine Learning (ML) and Artificial Intelligence (AI) are transformative fields that enable systems to learn patterns, make predictions, and automate decision-making using data and knowledge [3].

Machine Learning focuses on developing algorithms that build models from training data to optimize tasks such as classification, regression, and optimization.

Artificial Intelligence, on the other hand, is a broader field that generalizes these capabilities to encompass not only learning but also reasoning, planning, and knowledge representation. It involves sophisticated approaches to mimic human cognitive functions such as symbolic logic or heuristic search.

Together, they are revolutionizing various industries, from healthcare and finance to autonomous vehicles and personalized digital assistants, by enabling smarter, more efficient, and adaptive technologies.

In the financial domain, ML models analyze massive datasets. These can include market prices, transaction histories or risk indicators, to detect anomalies, forecast trends, and manage portfolios. AI augments these tasks with strategic reasoning and adaptive autonomy, driving advances in for example fraud detection or investment optimization. The uncertainty in financial and other real-world territories necessitates robust modeling of data distributions, a challenge met by probabilistic methods and advanced sampling techniques [4].

Data Representation in ML and AI

Data constitutes the foundational resource for ML and AI systems. It may exist as numerical records, time series, images, text documents, or relational graphs. The efficiency of learning and inference depend on how this data is represented. Common approaches include tabular datasets, feature vectors, relational graphs, and tensor networks, each suited for capturing structure, dependencies, and semantics within data.

Knowledge builds upon data by explicitly encoding recognized patterns, relationships, and rules. These are either uncovered through analysis or are previously contributed. This higher-level representation often takes the form of logical formulas, graphical models (such as Bayesian networks), or advanced tensor structures. Effectively, knowledge can be seen as data made explicit: enriched with well-defined dependencies, constraints, and connections. The representation chosen determines both the performance and expressiveness of ML/AI algorithms, especially when combining reasoning, prediction, and uncertainty quantification.

Sampling: Concepts and Role in ML/AI

Sampling is the process of drawing representative instances from a dataset or knowledge base, serving as a fundamental operation in machine learning and artificial intelligence workflows. It enables effective data handling and therefore helps facilitating efficient computations without compromising on representativeness. Sampling is pivotal in contexts such as training complex models, where it helps reduce computational load, making model building viable and scalable; or in decision-making processes, to simulate possible outcomes under uncertain conditions, supporting scenario analysis, planning, and risk assessment [5].

Simpler classical algorithms span brute-force, rejection and Markov Chain Monte Carlo (MCMC) methods. More advanced strategies like stratified sampling, systematic sampling, and cluster sampling can employed based on task requirements, data structure, and desired accuracy [6]. Additionally, in cases of imbalanced datasets, techniques like oversampling and undersampling ensure that minority classes are adequately represented, which is crucial for fair and effective model training.

Although a pivotal operation, with emerging dataset sizes/dimensions and model intricacies, it can be quite a challenge to perform efficient classical sampling.

Classical Sampling in Machine Learning: Challenges

Classical sampling algorithms, such as brute-force sampling, rejection sampling, and Markov Chain Monte Carlo (MCMC) methods; face significant barriers in contemporary machine learning applications. High-dimensional distributions with complex dependencies or sharp peaks result in slow mixing times and exponential resource scaling. For example, sampling from Bayesian networks with hundreds of variables or training deep generative models with multimodal posteriors often becomes computationally intractable [7]. These challenges are generally referred to as the 'curse of dimensionality', where the volume of the sampling space grows exponentially with the number of variables. Even state-of-the-art methods like Hamiltonian Monte Carlo or variational inference require trade-offs between approximation accuracy and computational cost, leaving room for fundamentally new computational paradigms.

Quantum Computing: Opportunities for Sampling

Quantum computing introduces novel strategies for sampling through unique principles such as superposition or entanglement, enabling new computational paradigms for sampling. Recent research demonstrates that quantum algorithms can sample from complex distributions with fewer resources than classical counterparts, particularly for problems with combinatorial structure or where classical simulation is intractable or even computationally prohibitive [8][9]. Quantum amplitude amplification, a generalization of Grover's search algorithm [10] enables quadratic speedups in identifying *target* solution states, and with repeated application also amplifying them within unstructured search spaces. Thus by encoding probability distributions into quantum states, this technique can efficiently sample from distributions that would be unfeasible for classical systems. Also, recent advances in quantum hardware, such as improved gate fidelities and coherence times suggest that near-term devices may soon support practical implementations [11]. However, practical deployment depends on circuit depth, noise resilience, hardware capabilities and seamless integration with classical machine learning workflows. These pose as critical challenges for quantum procedures to effectively overcome classical ones [12][13].

Thesis Objectives and Contributions

This thesis aims to bridge the gap between theory and practice in quantum-assisted sampling for machine learning. Our starting point is the ever becoming hardship of sampling high dimensional knowledge, and intractable classical solutions, with the solution being the use of quantum based methods, to overcome said issues. Quantum based methods become an option via a systematic methodology for generalizing the well used knowledge representations of logical connectives and probabilistic graphical models to exponential family distributions. These well defined distributions can be portrayed as tensor networks, from which the use of slice decomposition is enabling their representation as quantum states. The states can be manipulated with quantum operators, therefore opening the possibility of a quantum circuit representation. Implementation and simulation of amplification-based quantum sampling routines on said mapped distributions will be feasible.

After our process of generalizing knowledge representations, so quantum assisted sampling procedures can be used, the final step is to compare quantum sampling with classical baselines. Here we are quantifying speed, accuracy, and scalability, and analyzing theoretical speedup over classical counterparts. For precision and to have a landscape about the current state of quantum platforms, resource estimation is done for near-term quantum hardware. The procedure's empirical performance is assessed, providing actionable insights for algorithm deployment on NISQ platforms.

Thesis Structure

The remainder of this work is organized as follows:

- **Chapter 2** reviews foundational concepts of classical knowledge representations - logical connectives and probabilistic graphical models. Defines the formalism for mapping to exponential familiy distributions, with their tensor network representations.
- **Chapter 3** introduces quantum computing, defining quantum gates, measurements, and procedures, such as quantum amplitude amplification. Presents the mapping of decomposed tensor networks to quantum states and circuits.
- **Chapter 4** destribes my implementation of mapping a one dimensional logical formula to a quantum circuit through tensor network decomposition technique applied on its exponential family representation. Then the previously defined quantum measurement and amplitude amplification is performed as a quantum sampling procedure .
- **Chapter 5** compares the quantum sampling algorithm with classical counterparts for quantifying theoretical speedup. Benchmarks quantum sampling against classical methods, with analyzing scalability, and discussing practical deployment constraints.
- **Chapter 6** explores broader implications, limitations, and future research directions, finally concludes with a synthesis of contributions and an outlook on quantum sampling in AI.

Chapter 2

Foundations

2.1 Logical Connectives and Probabilistic Models

Artificial Intelligence (AI) and Machine Learning (ML) inherently involve sampling problems during training, learning, and optimization. Knowledge can be represented through different models, each with distinct advantages. Probabilistic graphical models such as Bayesian networks and Markov Random Fields (Markov Logic Networks), have become dominant in real-world applications. They can handle uncertainty and explicitly represent variable dependencies via graph structures [14]. In contrast, logical approaches represent knowledge as logical propositions. They use inference to draw deterministic conclusions, although recent developments now allow for probabilistic reasoning and sampling as well.
With extending the practical usage of logics, the field of Statistical Relational AI bridges the gap between representations, unifying logical relations with statistical models to handle uncertainty systematically. This synthesis, often termed *neuro-symbolic AI* [15], leverages the structured reasoning of logic and the uncertainty modeling of graphical models. For instance, logical rules can be embedded as soft constraints in probabilistic frameworks, enabling inference that balances symbolic precision with statistical robustness.
Both probabilistic and logical systems can be described by a set of properties, each called a categorical variable. A so-called *Atomic representation* of a system is described by the categorical variables X taking values x from a finite set:

$$[i] := \{0, 1, 2, \ldots, i-1\}$$

with cardinality i. We will call the variables by upper-case letters and the values by lower case letters, X_j and x_j respectively, with their indices serving as the connection between them. A *Factored representation* of the same system is the set of categorical variables X_j where $j \in [d]$, taking values in i_j. Thus system states are assignments to a set of variables. Global properties (e.g., overall probability or formula satisfaction) are built up as combinations of local factors or constraints involving subsets of these variables. A small example is in order so the various concepts and representation techniques are understandable and remain easy to follow throughout section 2 and 3.

A Bernoulli distribution is the discrete probability distribution of a random variable which takes the value '1' with probability p and the value '0' with probability $q = 1 - p$. Now consider binary variables $X_1, \dots X_n$, each representing a logical or probabilistic variable, with values $x_1, \dots x_n$, with all $x_i \in \{0, 1\}$. Suppose these variables are jointly independent Bernoulli random variables, with probabilities $P_1, \dots, P_n$ respectively. The joint distribution can be factorized as:

$$P(X_i = x_i \mid i \in \{1, \dots, n\}) = P_1(x_1)P_2(x_2)\dots P_n(x_n)$$

with each P_i being:

$$P_i(x_i) = p_i^{x_i}(1 - p_i)^{1-x_i}$$

thus:

$$P(x_1, x_2, \dots, x_n) = \prod_{i=1}^{n} p_i^{x_i}(1 - p_i)^{1-x_i}$$

Hence the joint distibution assumes a factored structure.

This structure admits a natural tensor representation, where variables correspond to tensor indices and their assignments to tensor entries. For example, a probability distribution over binary variables $X_1, \dots, X_n$ can be encoded as a rank-n tensor $\mathcal{T}[X_1, \dots, X_n]$, with each entry storing the probability of a specific joint assignment. Similarly, logical formulas map to tensors via one-hot encodings, where entries indicate formula satisfaction (1, TRUE) or violation (0, FALSE) of the given single logical connectives.
Tensor methods provide a unifying formalism for reasoning algorithms across probabilistic and logical frameworks. Marginalization corresponds to tensor contraction, while logical inference reduces to multilinear operations on formula-encoded tensors. This shared mathematical foundation enables seamless integration of probabilistic graphical models and symbolic logic, paving the way for scalable quantum sampling algorithms that exploit tensor network decompositions.

In the case of our example, marginalization would mean contraction over one of the factors of the joint distribution, for example on the k-th index ($k \in$

$\{1, 2, \ldots, n\}$):

$$P(x_1, x_2, \ldots, x_n) = \prod_{i=1}^{n-1} p_i^{x_i}(1-p_i)^{1-x_i} \sum_{x_k=0}^{1} p_k^{x_k}(1-p_k)^{1-x_k}$$

which for a Bernoulli distibution will result in:

$$\sum_{x_k=0}^{1} p_k^{x_k}(1-p_k)^{1-x_k} = 1$$

therefore:

$$P(x_1, x_2, \ldots, x_n) = \prod_{i=1}^{n-1} p_i^{x_i}(1-p_i)^{1-x_i}$$

which is the marginal distribution for a subset of variables.

2.1.1 Propositional Logic in AI

Propositional logic is a fundamental tool in artificial intelligence for representing and manipulating knowledge in a formal, symbolic manner. In this framework data is encoded as variables, while knowledge is encoded as a set of atomic propositions over these varibles, each of which can be either true or false. These atomic propositions can be combined using logical connectives such as AND ($\wedge$), OR ($\vee$), XOR ($\oplus$), NOT ($\neg$), IMPLIES ($\rightarrow$) and BIJECTION ($\leftrightarrow$) to form more complex statements or formulas, the symbolization of which is:

$$[[A \wedge B] \rightarrow C] = A \textit{ and } B \textit{ implies } C, \tag{2.1}$$

meaning that our premises are:

- **Formula:** $[[A \wedge B] \rightarrow C]$
- **Premise 1:** $X \rightarrow C$
- **Premise 2:** $[A \wedge B] = X$, where X serves as an intermediate variable
- **Conclusion:** C

Thus, to have the formula be true, we need the premises - defined by atomic (indivisible) statements - to be true.
Logical reasoning in AI often involves determining the satisfiability of a set of formulas, performing inference (e.g., deducing new facts from known ones), and checking

entailment between statements. For example, given a knowledge base consisting of rules and facts, an AI system can use logical inference mechanisms such as Modus Ponens or Resolution to derive new conclusions. Logical connectives can be mapped to indicator functions or binary variables, which facilitates their integration into probabilistic models. For instance, the truth value of a conjunction of variables, which is the formula itself, can be represented as the product of their indicator variables, i.e. the product of the individual indicator functions for the logical connectives. This way an overlap is present with the atomic representations defined in sect. 2.1, thus also admitting to a natural tensor representation. This mapping provides a bridge between symbolic logic and statistical modeling, enabling hybrid approaches that combine the strengths of both paradigms.

This symbolic approach underpins many classical AI systems, including expert systems, rule-based engines, and automated theorem provers [16].

2.1.2 Graphical Models: Bayesian and Markov Networks

Probabilistic graphical models (PGMs) provide a powerful framework for representing the conditional dependencies among random variables in complex systems. There are two principal types of probabilistic graphical models: Bayesian Networks and Markov Random Fields (networks of which is known as Markov Networks).

Bayesian networks are directed acyclic graphs (DAGs) in which each node represents a random variable, and each directed edge encodes a conditional dependency between variables. The structure of the graph captures the causal or informational relationships among the variables: a directed edge from node X_j to node X_i indicates that X_j is a direct parent (or cause) of X_i. The joint probability distribution over all variables in a Bayesian network factorizes according to the graph structure:

$$P(X_1, \dots, X_n) = \prod_{i=1}^{n} P(X_i \mid \mathrm{Pa}(X_i)) \tag{2.2}$$

where $\mathrm{Pa}(X_i)$ denotes the set of parent nodes of X_i. This factorization reflects the Markov property: each variable is conditionally independent of its non-descendants given its parents. This structure enables efficient inference and learning, especially when the graph is sparse.

Markov random fields are undirected graphs where nodes represent random variables and edges encode direct, symmetric interactions. The joint distribution is expressed as a product of potential functions over cliques (fully connected subsets of nodes):

$$P(X_1, \dots, X_n) = \frac{1}{Z} \prod_{C \in \mathcal{C}} \psi_C(X_C) \tag{2.3}$$

where $\mathcal{C}$ is the set of cliques, each ψ_C non-negative potential function over the variables in clique $C \in \mathcal{C}$, and Z is the partition function ensuring normalization. *MRFs* also can be defined through a partition function and an energy function:

$$P(X) = \frac{1}{Z} \exp\left(\sum_i w_i \phi_i(X)\right) \tag{2.4}$$

where w_i are weights and $\phi_i(X)$ are feature functions (often indicator functions of certain configurations). This energy based representation perfectly overlaps with the canonical exponential family form, where the exponent is a linear combination of sufficient statistics. Each potential function $\psi_C(X_C)$ can be written as an exponential of a sum of weighted features:

$$\psi_C(X_C) = \exp\left(\sum_{i \in F_C} w_i \phi_i(X_C)\right)$$

where F_C indexes the features associated with clique C. Substituting this into the product over cliques:

$$\prod_{C \in \mathcal{C}} \psi_C(X_C) = \exp\left(\sum_{C \in \mathcal{C}} \sum_{i \in F_C} w_i \phi_i(X_C)\right) = \exp\left(\sum_i w_i \phi_i(X)\right)$$

since each feature ϕ_i is associated with a clique.
Thus, the product-of-potentials form and the energy-based form are two views of the same distribution: the first emphasizes local factors, and the second emphasizes global energy or sufficient statistics.
The partition function can be defined as:

$$Z = \sum_X \prod_{C \in \mathcal{C}} \psi_C(X_C) = \sum_X \exp\left(\sum_i w_i \phi_i(X)\right)$$

thus ensuring normalization.
Both Bayesian networks and Markov networks can represent high-dimensional distributions compactly, capturing complex dependencies among variables. Many logical knowledge bases and rule systems can be embedded within graphical models, providing a bridge between symbolic and probabilistic reasoning. For example, logical rules can be encoded as hard or soft constraints in the potentials of a Markov network or as conditional probability tables in a Bayesian network.

Example: To showcase the differences between the two a small example is in order. Imagine a street, currently dry. Close to it, a well-kept garden, which has a sprinkler. The sky is kind of cloudy at the moment. Will the street be wet in the near future? The dependencies of course lie between the given nodes, as the 'wet street' variable is dependent on the fact, whether it is raining, or if the sprinkler is being used by the gardener, which of course also (somewhat) depends on the state of the weather. So our variables are:

- **A** - *Rain:* True/False
- **B** - *Sprinkler on:* True/False
- **C** - *Wet street:* True/False

Which admits to a factorization using a Bayesian network:

$$P(A, B, C) = P(A)P(B|A)P(C|A, B)$$

and with a Markov logic network:

$$P(A, B, C) = \frac{1}{Z}\psi_{CA}P(C, A)\psi_{CB}P(C, B)\psi_{BA}P(B, A)$$

where each ψ is a potential function (not necessarily normalized).

2.2 Exponential Family Distributions

2.2.1 Definition and Properties

The exponential family is a broad class of probability distributions that share a common functional (energy based) form, making them particularly amenable to statistical inference and learning [17][18]. A big group of distirbutions can be represented as exponential families, such as Bernoulli, Normal, Binomial, etc.; just like previously mentioned logical formulas 2.1.1 and probabilistic graphical models 2.1.2.

Canonical parameterization

A probability distribution $p(x \mid \theta)$ belongs to the exponential family if it can be parametrized as:

$$p(x) = \exp\{\langle\theta, \phi(x)\rangle - A(\theta)\} \tag{2.5}$$

where θ is the vector of canonical (or exponential) parameters which weight the features at a given state to calculate the respective probability. $\phi(x)$ is the sufficient statistics, a function of the data that encapsulates all the information relevant for inference about the canonical parameter parameter, usually a vector containing the features themselves. Finally, $A(\theta)$ is the cumulant function, (also called the log-partition function as it can be reshaped s.t.: $Z = exp\{-A(\theta)\}$) ensuring normalization, as per:

$$A(\theta) = \log \int_{\chi^m} \exp\langle\theta, \phi(x)\rangle \nu dx$$

where we presume that the integral is finite, so this defnition ensures that $p(x)$ is properly normalized. Thus the canonical parameterization of an exponential family is, as the name suggests, unique, characterized by the canonical parameters.

Mean parameterization

In addition to the canonical parameterization by canonical parameters and sufficient statistics, every exponential family admits a dual, alternative, so-called mean parameterization. The mean parameters μ_α are associated with the sufficient statistic ϕ_α as it is defined as the expected values of the sufficient statistics under the distribution:

$$\mu_\alpha = \mathbb{E}_p[\phi_\alpha(x)], \tag{2.6}$$

thus a mean parameter can be defined for each sufficient statistic, creating a set of all realizable mean parameters, known as the *marginal polytope* or *mean parameter space*:

$$\mathcal{M} := \{\mu \in \mathbb{R}^d \mid \exists\, p\ s.t.\ \mathbb{E}[\phi_\alpha(X)] = \mu_\alpha\} \tag{2.7}$$

A fundamental property of exponential families is that the mapping from canonical parameters θ to mean parameters μ is given by the gradient of the log-partition function:

$$\mu = \nabla_\theta A(\theta), \tag{2.8}$$

When switching from canonical to mean parameterization, the natural parameter θ is replaced with the mean parameter μ, using the gradient of the log-partition function to map between them. The sufficient statistics $\phi(x)$ remain unchanged, but the way the distribution is parameterized and interpreted changes fundamentally:

$$p(x) = \exp\{\langle\theta(\mu), \phi(x)\rangle - A(\theta(\mu))\} \tag{2.9}$$

The θ vector of canonical parameters, is now $\theta(\mu)$, showing not the 'effect' of the sufficient statistics, but the expectation value of those. The normalizing log-partition function turns from $A(\theta)$ to $A(\theta(\mu))$, which are conjugate duals. This duality underlies variational inference, maximum likelihood estimation, and moment-matching procedures. In practice, mean parameters often correspond to marginal probabilities (e.g., node and edge marginals in graphical models), and many inference algorithms (such as mean field and variational methods) operate directly in the mean parameter space, as we are dealing with expectation values, not weights. For example, marginalization can be understood as transforming from one parametrization to the other.

Key properties of exponential family distributions include:

- **Sufficient statistics**: The function $\phi(x)$ captures all information about the data relevant to parameter estimation.
- **Conjugacy**: Many exponential family distributions admit conjugate priors, meaning that it is often possible to select a prior distribution such that the resulting posterior distribution has the same functional form as the prior, just with updated parameters. Such conjugacy is simplifying Bayesian inference.
- **Tractable moments**: The moments and cumulants of an exponential family distribution can be computed as derivatives of the log-partition function $A(\theta)$, with the first derivative yielding the mean and higher-order derivatives corresponding to higher cumulants.
- **Generalization**: Many common distributions, such as the Bernoulli, multinomial, normal, and Poisson, and Markov Logic Networkscan be represented as exponential families.

In the context of AI and machine learning, exponential familiy representations can provide a general, unified framework that encompasses many commonly used distributions, such as probabilistic graphical models and logic-based systems. By choosing appropriate sufficient statistics (such as indicator functions for logical formulas), one can encode logical constraints and probabilistic dependencies within a single, tractable mathematical formalism.

2.2.2 MLNs as exponential families

Many logical knowledge bases, Markov Logic Networks (MLNs), and rule-based systems can be naturally expressed within the exponential family framework. In MLNs, for example, each logical formula ϕ_i is associated with a weight θ_i, and the probability of a world (i.e., a complete assignment of truth values) is given by:

$$P(X) \propto \exp\left(\sum_i \theta_i \phi_i(X)\right) \tag{2.10}$$

as seen in the energy based representation for MLNs 2.4. Here, $\phi_i(X)$ is an indicator function that evaluates to 1 if the formula is satisfied by X, and 0 otherwise. The weights θ_i determine the strength of each logical constraint: large positive values enforce hard constraints, while smaller values allow for soft, probabilistic reasoning.

This representation allows for the seamless integration of symbolic logic and statistical learning. Logical connectives can be encoded as sufficient statistics in the exponential family, and their weights can be learned from data. As the weights become large, the model approaches a purely logical system; as they decrease, the model becomes more probabilistic, capturing uncertainty and noise in the data.

After defining exponential families and presenting an easy example by the Markov Logic Networks, it would be time to have our example distribution of jointly independent Bernoulli variables mapped to an exponential family as well.
The distibution is:

$$P(x_1, x_2, \ldots, x_n) = \prod_{i=1}^{n} p_i^{x_i}(1-p_i)^{1-x_i}$$

where as we work with independent variables, the sufficient statistics and canonical variables are straightforward for the canonically parametrized exponential family:

$$P(x_1, x_2, \ldots, x_n) = \exp\left\{\sum_{i=1}^{n} \theta_i x_i - A(\theta)\right\}$$

- **Sufficient statistics:** are the counts of successes in our case, esentially the grounding of our formulas, i.e. when are we given a 1 as a result: $\phi(x_1, x_2, \ldots, x_n) = (x_1, x_2, \ldots, x_n)$,
- **Canonical parameters:** they are ought to be representing the *probabilities* of each distibution resulting in 1 or 0: $\theta_i = log\left(\frac{p_i}{1-p_i}\right)$.
- **Log-partition function:** should be normalizing the distribution, thus it should be $A(\theta) = \sum_{i=1}^{n} log(1 + e^{\theta_i})$

If we insert all of the above into the definition of the exponential family, we will get the Bernoulli distribution back, as per:

$$P(x_1, x_2, \ldots, x_n) = \exp\left\{\left[\sum_{i=1}^{n} log\left(\frac{p_i}{1-p_i}\right) \cdot x_i\right] - \left[\sum_{i=1}^{n} log(1 + e^{log\left(\frac{p_i}{1-p_i}\right)})\right]\right\}$$

With the first parantheses within the sum being the inner product of the sufficient statistics and canonical parameters, and the second the log-partition function. Let me open up the first parantheses to have:

$$[1.] = \exp\left\{\sum_{i=1}^{n}\left[log\left(\frac{p_i}{1-p_i}\right) \cdot x_i\right]\right\}$$

as it is the exponential of a sum, we can treat it as multiplying n-many exponentials together as such:

$$[1.] = \prod_{i=1}^{n} \exp\left\{\left[log\left(\frac{p_i}{1-p_i}\right)\cdot x_i\right]\right\}$$

and for each we can utilize that $e^{alog(b)} = b^a$:

$$[1.] = \prod_{i=1}^{n}\left(\frac{p_i}{1-p_i}\right)^{x_i}$$

And the second parantheses:

$$[2.] = \exp\left\{\sum_{i=1}^{n} - \left[log(1+e^{log\left(\frac{p_i}{1-p_i}\right)})\right]\right\}$$

we are dealing with the exponential of a sum again:

$$[2.] = \prod_{i=1}^{n}\exp\left\{-\left[log(1+e^{log\left(\frac{p_i}{1-p_i}\right)})\right]\right\}$$
$$[2.] = \prod_{i=1}^{n}\frac{1}{1+\left(\frac{p_i}{1-p_i}\right)}$$

Thus we have:

$$P(x_1, x_2, \ldots, x_n) = \prod_{i=1}^{n}\frac{\left(\frac{p_i}{1-p_i}\right)^{x_i}}{1+\left(\frac{p_i}{1-p_i}\right)}$$
$$P(x_1, x_2, \ldots, x_n) = \prod_{i=1}^{n}(1-p_i)\cdot\left(\frac{p_i}{1-p_i}\right)^{x_i}$$
$$P(x_1, x_2, \ldots, x_n) = \prod_{i=1}^{n}p_i^{x_i}(1-p_i)^{1-x_i}$$

which is the original form of the example distribution.

Alternatively the *mean parametrization* can also be utilized for defining exponential families. The mapping from canonical parameters θ to mean parameters μ is given by the gradient of the log-partition function:

$$\mu = \nabla_\theta A(\theta),$$

Using the equation above we see that the mean parameter μ_i for a given variable X_i should be:

$$\mu_i = \frac{\partial}{\partial\theta} log(1 + e^{\theta_i}) = \frac{e^{\theta_i}}{1 + e^{\theta_i}}$$

where $\theta_i = log\left(\frac{p_i}{1-p_i}\right)$:

$$\mu_i = \frac{\left(\frac{p_i}{1-p_i}\right)}{1 + \left(\frac{p_i}{1-p_i}\right)}$$

thus:

$$\mu_i = p_i$$

and the mean parameter vector:

$$\mu = \sum_{i=1}^{n} p_i$$

where if we use the definition for the mean parametrized exponential family:

$$P(x) = \exp\{\langle\theta(\mu), \phi(x)\rangle - A(\mu)\}$$

we will get our original distibution back:

$$P(x_1, x_2, \ldots, x_n) = \exp\left\{\left[\sum_{i=1}^{n} log\left(\frac{\mu_i}{1-\mu_i}\right) \cdot x_i\right] - \left[\sum_{i=1}^{n} log(1 + \left(\frac{\mu_i}{1-\mu_i}\right))\right]\right\}$$

$$P(x_1, x_2, \ldots, x_n) = \prod_{i=1}^{n} \mu^{x_i}(1-\mu)^{1-x_i}$$

where $\mu_i = p_i$

2.3 Tensor Networks

2.3.1 Tensor Network Basics

A *tensor* is a multi-dimensional array generalizing scalars (0th order), vectors (1st order), and matrices (2nd order) to arbitrary dimensions. Formally, an nth-order tensor $\mathcal{T} \in \mathbb{R}^{d_1 \times \cdots \times d_n}$ has n indices, each ranging over dimensions $d_1, \ldots, d_n$. Tensors enable compact representation of high-dimensional functions, such as joint probability distributions over many variables.

A *tensor network* is a structured factorization of a high-order tensor into a collection of lower-order tensors connected via contractions over shared indices. Graphically, nodes represent tensors, and edges denote contracted indices.

Key operations in tensor networks include:

- **Contraction**: Summing over shared indices, e.g., $\mathcal{C}[i, j] = \sum_k \mathcal{A}[i, k]\mathcal{B}[k, j]$ for matrix multiplication.
- **Decomposition**: Approximating $\mathcal{T}$ as a network/sequence of simpler (i.e. lower dimensional) tensors (like Canonical-Polyadic (CP), Matrix Product State (MPS), or tensor train (TT)).
- **Normalization**: Enforcing constraints (e.g., non-negativity) to represent valid probability distributions.

Tensor networks excel at capturing locality and hierarchy in data. For example, a tree tensor network (TTN) mirrors the structure of a Bayesian network, with each node representing a conditional probability table and edges encoding variable dependencies.

2.3.2 Tensor Networks for Probabilistic Models

The joint probability distribution encapsulated in a graphical model can be encoded as a tensor where each entry $\mathcal{T}[x_1, \ldots, x_n]$ stores $P(X_1 = x_1, \ldots, X_n = x_n)$. Tensor networks factorize this high-dimensional tensor into localized components reflecting the model's conditional independence structure.

Example: Bayesian Network as a Tensor Network
Consider a Bayesian network over binary variables X_1, X_2, X_3 with edges $X_1 \to X_2$ and $X_2 \to X_3$. The joint distribution is:

$$P(X_1, X_2, X_3) = P(X_1)P(X_2|X_1)P(X_3|X_2) \tag{2.11}$$

Which factorizes to a tensor network:

$$\mathcal{T}[X_1, X_2, X_3] = \sum_Y \mathcal{A}[X_1]\mathcal{B}[X_1, X_2, Y]\mathcal{C}[X_2, X_3, Y] \tag{2.12}$$

where Y is an auxiliary index connecting the two conditional tensors $\mathcal{B}[X_1, X_2, Y]$ and $\mathcal{C}[X_2, X_3, Y]$, with $\mathcal{A}[X_1]$ being the prior tensor to X_1. The conditional tensors have been added an additional so-called bond index Y, which serves as a virtual bond indexing the possible channels (i.e. connection) between X_2 and its neighbours X_1 and X_3, by which the dependency can be communicated through. It is not a probabilistic variable, and its dimension is the number of possible states being passed along, in our case the possible assignments to X_2 (so for binary variables, the dimension should be 2 as $X_2 \in \{0, 1\}$)

Example: Markov Random Field as a Tensor Network
Consider a Markov random field (MRF) over binary variables $X = \{X_1, X_2, X_3\}$, with direct edges between $\{X_1, X_2\}$ and $\{X_2, X_3\}$. These are the clicques contained in the graph. The joint distribution is:

$$P(X) = \frac{1}{Z}\psi_{12}(X_1, X_2)\psi_{23}(X_2, X_3) \tag{2.13}$$

This corresponds to a tensor network:

$$\mathcal{T}[X_1, X_2, X_3] = \sum_{Y} \psi_{12}[X_1, X_2, Y]\psi_{23}[Y, X_2, X_3] \tag{2.14}$$

where Y is an auxiliary index connecting the two clique tensors. This meets the Tensor Network representation of Propositional Logical formulas as well, where we can define the unique Logical connectives through the $\psi_{X_n,X_m,Y}$ functions, with X_n, X_m being the variables for the connective and the Y should be the 'ancilla' connecting the connectives to have the Logical formula in the end.

Key Applications relevant to Machine Learning frameworks:

- **Marginalization**: Marginalizing over variables—to compute $P(X_i)$ or any subset of marginals—involves summing (contracting) over all indices of the tensor network except those corresponding to the target variable(s). In traditional representations, this would require summing over an exponential number of configurations. However, when the model is represented as a tree tensor network (TTN) or similarly structured tensor network (e.g., MPS/TTN for chain/tree-like dependencies), contractions can be performed locally and in sequence, resulting in an overall computational cost that scales linearly (or at most polynomially) with the number of variables n.

- **Sampling**: Sampling from the joint distribution can be realized efficiently within the tensor network framework. In Bayesian networks, this reduces to ancestral sampling: start at the root nodes, sample values according to their local tensors (conditional probabilities or potentials), and propagate these values down the network, sequentially sampling each variable conditioned on its parents. For a directed acyclic tensor network, this is equivalent to performing a sequence of local contractions and probabilistic selections, efficiently navigating the high-dimensional sample space by leveraging the graphical structure.

- **Learning**: Parameter estimation, particularly maximum likelihood learning, is naturally phrased as tensor factorization in this context. The goal is to decompose the observed joint distribution tensor into a product of lower-order tensors (factors), such that their contraction approximates the data tensor as closely as possible. Algorithms like alternating least squares (ALS) iteratively update one tensor factor at a time, holding the others fixed, to minimize reconstruction error. This approach generalizes to learning in graphical models, tensor decomposition of observed statistics, and parameter estimation in large exponential family models where full enumeration and direct optimization would be infeasible.

2.4 Tensor Network Representation of Exponential Families

Exponential family distributions, due to their structured parameterization and sufficient statistics, are naturally suited for representation as tensor networks. This correspondence enables efficient manipulation, marginalization, and sampling—crucial for high-dimensional probabilistic models and for mapping to quantum circuits.

2.4.1 Slice Tensor Decomposition

A central technique for representing high-order tensors arising from exponential family models is *slice tensor decomposition*. In this approach, a high-dimensional tensor $\mathcal{T}[X_1, \ldots, X_n]$ encoding the joint distribution is factorized into a sum of lower-rank tensors (slices) along one or more modes:

$$\mathcal{T}[X_1, \ldots, X_n] = \sum_{k=1}^{r} \lambda_k \, \mathcal{A}_k[X_1] \otimes \mathcal{B}_k[X_2, \ldots, X_n] \tag{2.15}$$

where λ_k are scalar coefficients, and $\mathcal{A}_k$, $\mathcal{B}_k$ are subtensors or vectors corresponding to particular slices. This decomposition preserves the conditional independence structure of the underlying graphical or logical model and allows for efficient storage and computation, especially when the tensor admits a low-rank structure.

Slice decomposition is particularly powerful for models with factorizable sufficient statistics, such as those arising logical formulas or probabilistic (graphical) models, where each logical formula or clique potential can be associated with a tensor slice. The resulting network (between the slices) can then be contracted, such asmultiplied and summed over shared indices, to recover marginals or conditionals.

2.4.2 Operational Mapping: Step-by-Step Example

To illustrate, consider a simple exponential family model over three binary variables X_1, X_2, X_3. The joint distribution can be encoded as a rank-3 tensor $\mathcal{T}[X_1, X_2, X_3]$. Suppose the model factorizes as:

$$\mathcal{T}[X_1, X_2, X_3] = \sum_{k=1}^{r} \mathcal{S}_k[X_1] \cdot \mathcal{U}_k[X_2] \cdot \mathcal{V}_k[X_3] \tag{2.16}$$

where each $\mathcal{S}_k$,$\mathcal{U}_k$, $\mathcal{V}_k$ is a vector (or slice) over its respective variable, and r is the decomposition rank. This format is equivalent to the canonical polyadic (CP) decomposition and is especially efficient when r is small compared to the full tensor size.

In practice, such decompositions can be obtained via algebraic methods (e.g., alternating least squares) or by exploiting the structure of the model (e.g. realizing the factored representation and using the factor graph, or logical formulae). The resulting tensor network can then be contracted to compute marginals, conditionals, or to generate samples.

Chapter 3
Quantum Sampling Algorithms

With the previous chapter containing classical representations, decomposition techniques and practices, this chapter will provide insight to quantum algorithms and methods. Basics of quantum circuits, with gates and measurements will be the starting point of getting acquainted with the notations and inner workings of a quantum algorithm. The main component of our procedure, amplitude amplification, will be defined just afterwards. At the end of the chapter I will turn briefly to slice tensor decomposition methodology, extending the definition from sect. 2.4.1. This will provide a path for mapping classical representations 2.1 to measurable quantum states.

3.1 Quantum Gates, Circuits, and Measurement

Quantum gates, circuits, and measurements together provide the operational foundation for gate-based algorithms. Gates manipulate the amplitudes and phases of quantum states, circuits implement complex transformations, and measurement extracts classical information. This formalism, combined with parallelism, entanglement and superposition is enabling quantum algorithms to outperform their classical counterparts in sampling, search, and inference [19].

This section summarizes the essential elements relevant for algorithms used in the experiments, such as amplitude amplification and the representation of classical knowledge bases as quantum states.

3.1.1 Qubit States and Quantum Registers

A single qubit is described by a state vector in a two-dimensional Hilbert space,

$$|\psi\rangle = v_0 |0\rangle + v_1 |1\rangle , \tag{3.1}$$

where v_0 and v_1 are complex amplitudes satisfying $|v_0|^2 + |v_1|^2 = 1$; or a density matrix,

$$\rho = |\psi\rangle \langle\psi|$$

This is a single qubit pure state. The basis states $|0\rangle$ and $|1\rangle$ can be represented as column vectors:

$$|0\rangle = \begin{bmatrix}1\\0\end{bmatrix}, \quad |1\rangle = \begin{bmatrix}0\\1\end{bmatrix}.$$

A probabilistic mixture of such pure states are called mixed states, described by a density matrix, denoted as:

$$\rho = \sum_i p_i |\psi\rangle \langle\psi|$$

where $p_i \leq 0$ and $\sum_i p_i = 1$, with each $|\psi\rangle$ being a pure state. Mixedness is measured by the trace of the squared density operator, which for pure states result in one, but for mixed states it should be less than 1. Thus by calculating $Tr(\rho^2) \leq 1$, we can se how mixed our state is.

For multi-qubit systems, the overall state space is the tensor product of the individual qubit Hilbert spaces. For a two-qubit system (with qubits X and Y), a general pure state can be written as

$$|\psi\rangle = v_{00}|00\rangle + v_{01}|01\rangle + v_{10}|10\rangle + v_{11}|11\rangle,$$

where each basis element $|ij\rangle$ is understood as the tensor product $|i\rangle_X \otimes |j\rangle_Y$ (often abbreviated as $|XY\rangle$).

Another important classification is done by the separability of the state. If the coefficients factor as $v_{ij} = a_i b_j$, then the state is *separable* and can be written as a tensor product of single-qubit states: $|\psi\rangle = |\phi\rangle_X \otimes |\varphi\rangle_Y$. However, in quantum systems, there also exist *entangled states* that cannot be written as such a product. For example, the Bell state

$$|\Psi^+\rangle = \frac{1}{\sqrt{2}}(|01\rangle + |10\rangle)$$

is a prototypical entangled state: its overall two-qubit properties cannot be described by considering either qubit separately. Entanglement thus reflects the intrinsically quantum correlations present in the joint tensor product state, which are fundamental to quantum information processing and not captured by classical probability or separable states.

3.1.2 Quantum Gates: Basic Building Blocks

Quantum gates are unitary operations acting on one or more qubits. These unitary operations are represented as unitary matrices. A gate acting on n qubits is a $2^n \times 2^n$ unitary matrix. An invertible complex square matrix $\mathbf{U}$ is a unitary matrix, when its inverse $\mathbf{U^{-1}}$ is equal to its conjugate transpose $\mathbf{U}^+$. Thus all quantum operations

defined by gates are reversible, as the matrices defining these gates are invertible. They generalize classical logic gates but can create superposition and entanglement, enabling quantum parallelism.
Some important examples are:

Single-Qubit Gates:

- **Pauli-X (NOT) Gate:** Flips $|0\rangle$ to $|1\rangle$ and vice versa.

$$\hat{X} = \begin{bmatrix} 0 & 1 \\ 1 & 0 \end{bmatrix}$$

- **Pauli-Y and Pauli-Z Gates:** $\hat{Y}$ combines a bit and phase flip; $\hat{Z}$ applies a phase flip to $|1\rangle$.

$$\hat{Y} = \begin{bmatrix} 0 & -i \\ i & 0 \end{bmatrix}, \quad \hat{Z} = \begin{bmatrix} 1 & 0 \\ 0 & -1 \end{bmatrix}$$

- **Hadamard (H) Gate:** Creates superposition. When applied to $|0\rangle$, it yields $\frac{|0\rangle+|1\rangle}{\sqrt{2}}$, which is the uniform superposition.

$$\hat{H} = \frac{1}{\sqrt{2}} \begin{bmatrix} 1 & 1 \\ 1 & -1 \end{bmatrix}$$

- **Phase Gates:** modifies the phase of the quantum state, but the measurement probabilities stay.

$$\hat{P}(\varphi) = \begin{bmatrix} 1 & 0 \\ 0 & e^{i\varphi} \end{bmatrix}$$

- **Rotation Gates:** $\hat{R}_x(\theta)$, $\hat{R}_y(\theta)$, and $\hat{R}_z(\theta)$ rotate the qubit state around the respective axes by angle θ.

$$\hat{R}_{P_g}(\theta) = e^{-i\hat{P}_g\theta/2} = \cos\frac{\theta}{2} \cdot \hat{1} - i\sin\frac{\theta}{2} \cdot \hat{P}_g$$

where P_g are the possible Pauli gates $(X,\ Y,\ Z)$.

Multi-Qubit Gates:

- **SWAP Gate:** Exchanges the states of two qubits.

$$\hat{U}_{Swap} = \begin{bmatrix} 1 & 0 & 0 & 0 \\ 0 & 0 & 1 & 0 \\ 0 & 1 & 0 & 0 \\ 0 & 0 & 0 & 1 \end{bmatrix}$$

- **CNOT (Controlled-NOT) Gate:** A two-qubit gate that flips the target qubit if the control qubit is $|1\rangle$. Essential for generating entanglement.

$$\hat{U}_{CNot} = \begin{bmatrix} 1 & 0 & 0 & 0 \\ 0 & 1 & 0 & 0 \\ 0 & 0 & 0 & 1 \\ 0 & 0 & 1 & 0 \end{bmatrix}$$

  Also, it can be stylized as $C\hat{X}$ as the *Not* operation applied to the target qubit is a *Pauli-X* gate.

- **Toffoli (CCNOT) Gate:** A three-qubit gate; flips the third (target) qubit if both control qubits are $|1\rangle$. Important for universal reversible computation and error correction.

$$\hat{U}_{Toffoli} = \begin{bmatrix} 1 & 0 & 0 & 0 & 0 & 0 & 0 & 0 \\ 0 & 1 & 0 & 0 & 0 & 0 & 0 & 0 \\ 0 & 0 & 1 & 0 & 0 & 0 & 0 & 0 \\ 0 & 0 & 0 & 1 & 0 & 0 & 0 & 0 \\ 0 & 0 & 0 & 0 & 1 & 0 & 0 & 0 \\ 0 & 0 & 0 & 0 & 0 & 1 & 0 & 0 \\ 0 & 0 & 0 & 0 & 0 & 0 & 0 & 1 \\ 0 & 0 & 0 & 0 & 0 & 0 & 1 & 0 \end{bmatrix}$$

  Sometimes it is stylized as $MC\hat{X}$, or *multi-controlled-$\hat{X}$*, as it applies an $\hat{X}$ gate, which depends on 2 control qubits.

Using quantum gates one can realize universal sets of quantum gates. These are sets of gates to which any operation possible on a quantum computer can be reduced. Meaning that an arbitrary quantum operation or even other gates can be relized through the member of such a set, when applying them in a given sequence. Famous examples may be:

- $\{\hat{U}_{CNot}, \hat{H}, \hat{S}\} + \hat{T}$ gate. The first set is called the Clifford set, which, when extended with the $\hat{T}$ gate, gives a uniform set. $\hat{S}$ and $\hat{T}$ gates are specific Phase-shift gates; $\hat{S} = P(\frac{\pi}{2})$ and $\hat{T} = P(\frac{\pi}{4})$ respectively.
- Rotation operators $\{\hat{R}_x(\theta), \hat{R}_y(\theta)$, and $\hat{R}_z(\theta)\}$, $\hat{U}_{CNot}$ and the Phase-shift gate $P(\varphi)$

3.1.3 Quantum Circuits

A quantum circuit is a sequence of quantum gates applied to qubits, typically followed by measurement. Circuits are often depicted as diagrams, with qubits as horizontal lines and gates as symbols acting on these lines. For example, the circuit for creating a Bell state applies a Hadamard gate to the first qubit, followed by a CNOT with the first as control and the second as target, as seen in the figure below 3.1.

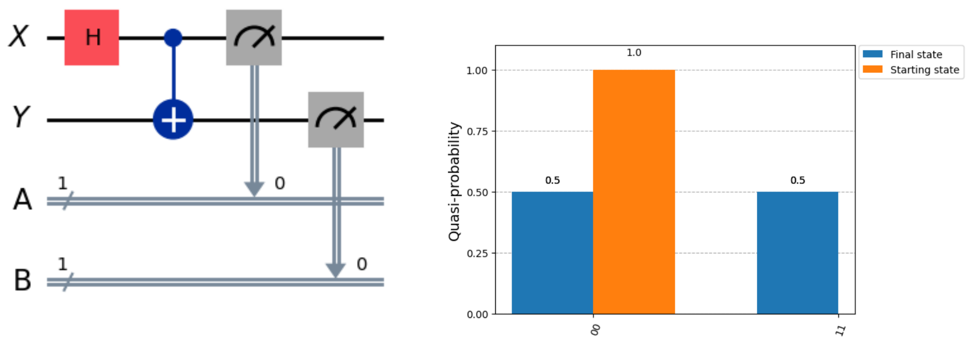

(a) Entangling circuit (b) Result of circuit measurement

Figure 3.1: X and Y denote the quantum bits, which we wil refer as variable qubits. A and B are the classical registers, which we project our measurement results to. The variable qubits posess the state $|0\rangle$, as seen in the orange histograms in 3.1b The gates are a Hadamard gate (*red*), and a Controlled-NOT (*blue*). The circuit results in $\hat{U}\,|00\rangle = C\hat{X}_{XY}\hat{H}_X\,|00\rangle = C\hat{X}_{XY}\frac{1}{\sqrt{2}}(|00\rangle + |10\rangle) = \frac{1}{\sqrt{2}}(|00\rangle + |11\rangle)$, which is depicted in the same subfigure as the starting state distibution, but via the blue histograms.

The action of a circuit on an initial state $|\psi_0\rangle$ is a sequence of unitary transformations:

$$|\psi_{\text{final}}\rangle = U_k \cdots U_2 U_1\,|\psi_0\rangle\,,$$

where each U_i is a quantum gate.

3.1.4 Measurement in Quantum Mechanics

A measurement is the testing or manipulation of a physical system to yield a numerical result. In quantum mechanics it is when a quantum state collapses to a classical outcome. Given an observable $\hat{O}$ we can write the spectral decomposition as:

$$\hat{O} = \sum_i o_i \mathbb{P}_i$$

where o_i are real numbers and $\mathbb{P}_i$ are projection operators to the eigenspace corresponding to the eigenvalue o_i.

Given a state ρ, when we measure the observable $\hat{O}$, we obtain one of its eigenvalues o_i as an outcome. The probability p_i and the state after measurement ρ_i are:

$$\begin{aligned} p_i &= Tr(\mathbb{P}_i \rho) \\ \rho_i &= \frac{1}{p_i} \mathbb{P}_i \rho \mathbb{P}_i \end{aligned}$$

For multi-qubit systems, measurement projects the state onto one of the basis vectors $|k\rangle$, with probability $|v_k|^2$.
An easy example is the single qubit superposition state from eq 3.1:

$$\rho = |\psi\rangle \langle\psi| = \frac{1}{2} \begin{pmatrix} 1 & 1 \\ 1 & 1 \end{pmatrix}$$

and the Pauli-Z as an observable ($\hat{O} = \hat{Z}$), admitting to the spectral decomposition:

$$\hat{O} = \hat{Z} = \begin{pmatrix} 1 & 0 \\ 0 & 1 \end{pmatrix} = o_0 \mathbb{P}_0 + o_1 \mathbb{P}_1 = 1 \cdot \begin{pmatrix} 1 & 0 \\ 0 & 0 \end{pmatrix} + 1 \cdot \begin{pmatrix} 0 & 0 \\ 0 & 1 \end{pmatrix}$$

Thus when we measure the projector $\mathbb{P}_0$:

$$\begin{aligned} p_0 &= Tr(\mathbb{P}_0 \rho) = \frac{1}{2} Tr \begin{pmatrix} 1 & 0 \\ 0 & 0 \end{pmatrix} \begin{pmatrix} 1 & 1 \\ 1 & 1 \end{pmatrix} = \frac{1}{2} \\ \rho_0 &= \frac{1}{p_0} \mathbb{P}_0 \rho \mathbb{P}_0 = 2 \cdot \begin{pmatrix} 1 & 0 \\ 0 & 0 \end{pmatrix} \frac{1}{2} \begin{pmatrix} 1 & 1 \\ 1 & 1 \end{pmatrix} \begin{pmatrix} 1 & 0 \\ 0 & 0 \end{pmatrix} = \begin{pmatrix} 1 & 0 \\ 0 & 0 \end{pmatrix} \end{aligned}$$

and the projector $\mathbb{P}_1$:

$$\begin{aligned} p_1 &= Tr(\mathbb{P}_1 \rho) = \frac{1}{2} Tr \begin{pmatrix} 0 & 0 \\ 0 & 1 \end{pmatrix} \begin{pmatrix} 1 & 1 \\ 1 & 1 \end{pmatrix} = \frac{1}{2} \\ \rho_0 &= \frac{1}{p_0} \mathbb{P}_0 \rho \mathbb{P}_0 = 2 \cdot \begin{pmatrix} 0 & 0 \\ 0 & 1 \end{pmatrix} \frac{1}{2} \begin{pmatrix} 1 & 1 \\ 1 & 1 \end{pmatrix} \begin{pmatrix} 0 & 0 \\ 0 & 1 \end{pmatrix} = \begin{pmatrix} 0 & 0 \\ 0 & 1 \end{pmatrix} \end{aligned}$$

The outcome is inherently probabilistic, a fundamental departure from classical computation.

Entanglement and Measurement: Measurement on one qubit of an entangled pair instantaneously determines the outcome of the other, a phenomenon with no classical analog. For example, measuring one qubit of the Bell state $(|00\rangle + |11\rangle)/\sqrt{2}$ collapses the other qubit to the same value, with causality being preserved, since no information is being transmitted during the measurement process (which is called the no communication theorem [20]). It will be utilized in my implementation to enable backpropagation as a learning procedure.

3.2 Amplitude Amplification: Theory and Practice

Amplitude amplification is a quantum algorithmic technique that generalizes Grover's search [10], providing a quadratic speedup for the identification or sampling of target states in an unstructured search space. The power of amplitude amplification lies in its ability to systematically increase the probability amplitude associated with desirable outcomes, making it a central primitive for quantum-enhanced sampling in machine learning.

3.2.1 Grover's Algorithm and Generalizations

Grover's algorithm is the canonical example of amplitude amplification. In the classical setting, searching for a marked item in an unsorted database of size N requires, on average, $O(N)$ queries, as with random selection, each and every item would have a $\frac{1}{N}$ probability of finding, Grover's quantum approach reduces this to $O(\sqrt{N})$ by exploiting quantum superposition and entanglement.

The algorithm operates in an N-dimensional Hilbert space $\mathcal{H}$, where each basis state $|k\rangle$ encodes a possible solution. A Boolean oracle function $\chi : \{0,1\}^n \to \{0,1\}$ identifies target states. The oracle operator $\mathbf{O}$ applies a phase flip to these states, while the diffusion operator $\mathbf{D}$ amplifies their amplitudes.

Brassard et al. [21] extended Grover's idea to arbitrary initial states and general quantum algorithms, formalizing the amplitude amplification operator:

$$\mathbf{Q} = -\mathcal{A}\mathbf{S}_0\mathcal{A}^{-1}\mathbf{S}_\chi$$

where $\mathcal{A}$ prepares the initial state over n qubits ($|\psi\rangle = \mathcal{A}|0\rangle^{\otimes n}$), $\mathbf{S}_\chi$ flips the phase of good states, and $\mathbf{S}_0$ flips the phase of the all-zero state. Repeated application of $\mathbf{Q}$ rotates the quantum state in the two-dimensional subspace spanned by the good and bad components, continuously increasing the probability of measuring a good state.

3.2.2 Oracle and Diffusion Operator Design

The effectiveness of amplitude amplification hinges on the careful design of the oracle and diffusion operators.

Oracle Operator O: The oracle is a unitary operator that marks the set of good states by flipping their phase. For a basis state $|k\rangle$, in the state space $\mathcal{S} := \{|k\rangle\}_{k=0}^{N-1}$,

$$\mathbf{O}|k\rangle = (-1)^{\chi(k)}|k\rangle$$

where $\chi(k) = 1$ for good states and 0 otherwise. In practical terms, the oracle is implemented as a quantum circuit that evaluates the Boolean function χ and applies a controlled-Z or multi-controlled Toffoli gate to flip the phase of the target states. For simple logical connectives, such as AND or OR, the circuit construction is straightforward. For more complex constraints, the circuit depth increases, but the principle remains the same: the oracle must be a reversible, unitary operation that encodes the solution set into phase flips. Of course here we assume that we know what the *target* state and our state space is, but with an unknown *target*, the procedure requires some help, in the form of either a sensing algorithm, or an additional ancilla on which a phase oracle can be applied, but this will not be neccesary with our conditions.

Diffusion Operator D: The diffusion operator, or "inversion about the mean," amplifies the amplitudes of the marked states. For an initial state $|\psi\rangle = \mathcal{A}|0\rangle$, the diffusion operator is

$$\mathbf{D} = 2|\psi\rangle\langle\psi| - \mathbb{1}$$

This operator reflects the quantum state about the initial state vector. In the special case where $|\psi\rangle$ is the uniform superposition, $\mathbf{D}$ can be implemented by Hadamard gates, a phase flip on $|0\rangle$, and another round of Hadamards. For non-uniform initial states, the diffusion operator is constructed by applying the inverse of the state preparation circuit, a phase flip on $|0\rangle$, and then re-applying the state preparation.

Geometric Interpretation: The interplay between the oracle and diffusion operators can be visualized as a sequence of reflections in a two-dimensional subspace. With a projection operator emerging from the definition of $\mathbf{O}$;

$$\mathcal{P} := \sum_{\chi(k)=1} |k\rangle\langle k|$$

defining the good and bad subspaces respectively:

$$\mathcal{H}_G := Im(\mathcal{P}) = span\{|k\rangle \in \mathcal{S}_{op} \mid \chi(k) = 1\}$$
$$\mathcal{H}_B := Ker(\mathcal{P}) = span\{|k\rangle \in \mathcal{S}_{op} \mid \chi(k) = 0\}$$

If we adopt the convention of $\sum'$ for summation over the solution states, and $\sum''$ for summation over the non-solutions, we can define normalized states as such:

$$|x_G\rangle = \sqrt{\frac{1}{M}} \sum_x{}' |x\rangle$$
$$|x_B\rangle = \sqrt{\frac{1}{N-M}} \sum_x{}'' |x\rangle$$

where **N** is the number of states (2^n for n qubits) and **M** is the number of solution states. Thus the initial state can be realized as:

$$|\psi\rangle = \sqrt{\frac{N-M}{N}}\,|x_B\rangle + \sqrt{\frac{M}{N}}\,|x_G\rangle = \cos\left(\frac{\alpha}{2}\right)|x_B\rangle + \sin\left(\frac{\alpha}{2}\right)|x_G\rangle$$

This is then a two-dimensional subspace spanned by the vectors $|x_G\rangle$ and $|x_B\rangle$. It is closed under the action of **Q**. The oracle reflects the state about the bad subspace (i.e. the $|x_B\rangle$ register), while the diffusion operator reflects about the initial state.

The composition of these two reflections is a rotation by an angle of α towards the good subspace. This geometric process underlies the quadratic speedup of amplitude amplification, which will be cleared in the next section, where coming from the geometric interpretation we can calulate the updated amplitude of our state with each rotation, therefore we are able to have a value for the number of rotations needed for maximum amplification.

3.2.3 Parameter Update Interpretation

The action of the amplitude amplification operator **Q** can be interpreted as two reflections – once over the bad states, and then over the average amplitude of our states (i.e. the register itself in the two-dimensional subspace) – which geometrically is a rotation in the two-dimensional subspace of the Hilbert space spanned by the projections of the initial state onto the good and bad subspaces. The initial state can be written as

$$|\psi\rangle = \sin\left(\frac{\alpha}{2}\right)|\psi_g\rangle + \cos\left(\frac{\alpha}{2}\right)|\psi_b\rangle$$

where $|\psi_g\rangle$ and $|\psi_b\rangle$ are normalized projections onto the good and bad subspaces respectively, ultimately resulting in the 2 dimensional subspace, which I will refer to as H_ψ. The result of said rotations in H_ψ can be depicted as seen in figure 3.2a. As the state is stable under the action of **Q**, the rotaion angle of $\frac{\alpha}{2}$ is given. Thus, Each application of **Q** rotates the state by $2 \cdot \frac{\alpha}{2} = \alpha$, such that after k iterations,

$$\mathbf{Q}^k\,|\psi\rangle = \sin\left((2k+1)\frac{\alpha}{2}\right)|\psi_g\rangle + \cos\left((2k+1)\frac{\alpha}{2}\right)|\psi_b\rangle$$

The probability of measuring a good state thus increases quadratically with the number of iterations, reaching a maximum when $(2k+1)\frac{\alpha}{2} \approx \pi/2$, resulting in:

$$k = \lfloor \frac{\pi}{4}\sqrt{\frac{1}{P_g^0}} \rfloor \tag{3.2}$$

meaning, that after exactly k rotations we will have a maximum amplification of our state. This repeated applications, each resulting in a rotation with angle α, can

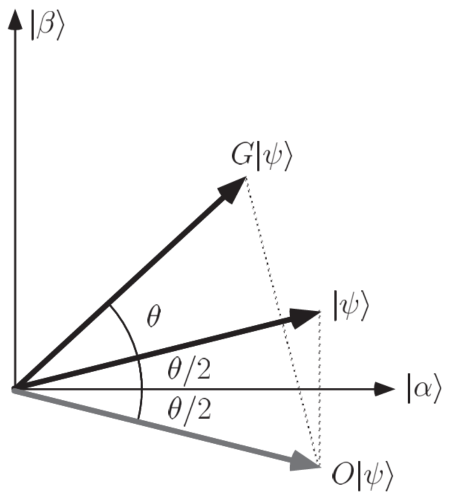

(a) Grover rotation in the 2 dimensional subspace H_ψ

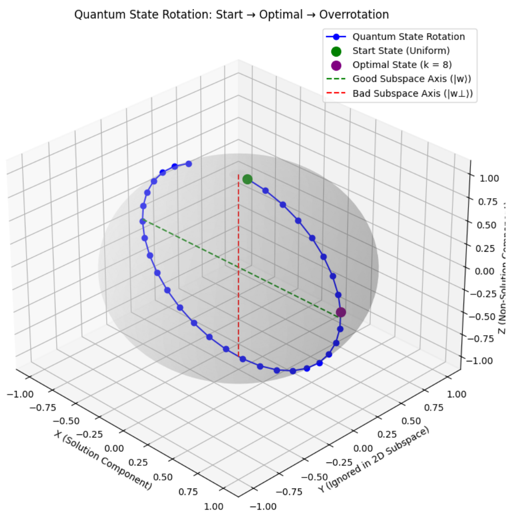

(b) Repeated applications in the complete state space

be seen in a 3-dimensional representation in figure 3.2b, where the axes are the *bad* ($|\psi_b\rangle$) and *good* ($|\psi_g\rangle$) states, spanning H_ψ. It is also visible now, that compared to classical algorithms, that can reach a time-depth of $\mathcal{O}(\frac{1}{P}) = \mathcal{O}(N)$, with amplitude amplification we are able to reach $\mathcal{O}(\sqrt{\frac{1}{P}}) = \mathcal{O}(\sqrt{N})$, which is a quadratic speedup for quantum algorithms over classical.

3.2.4 Scalability and Simulator Limitations

The scalability of amplitude amplification is determined by the complexity of the oracle and diffusion operators, the number of required rotations k, as well as the available quantum resources. For simple logical connectives and small models, both operators can be implemented with shallow circuits, and the algorithm can be simulated efficiently on classical hardware. In this case allocating one qubit for each variable (node), we have n number of quantum registers, each followed by a constant number of gates representing the structure (i.e. the probabilities encode in amplitudes). Thus the state preparation can be done with a circuit of depth $\mathcal{O}(c_0 n)$, where c_0 represents the constant number of gates per variable qubit. As we are working around binary valued variables we only need a simple gate sequence for the oracle ($\hat{Z}$ or $\hat{X}\hat{Z}\hat{X}$). The diffusion operator would admit to the sequence $\mathcal{A}^{-1}CC\hat{Z}\mathcal{A}$. Thus k rotations would result in a depth of $\mathcal{O}(k \cdot (2c_0 n))$, where we dropped the constant number of gates unrelated to n. Thus the whole process requires a circuit of depth

$\mathcal{O}((1+2k)\cdot c_0 n)$ which is $\approx \mathcal{O}(n+kn)$. Thus we have a state preparation of $\mathcal{O}(n)$ plus the amplification of $\mathcal{O}(kn)$. For more complex logical formulas or high-dimensional models, the circuit depth and qubit count increases. We need more ancillas for the structure encoding, and with more qubits, and possibly lower probability for achieving the target, a higher number of Grover iterations would be needed. This means that inherently, more gates are involved in both the state preparation and the amplification procedures. Therefore classical simulation becomes intractable.

In this work, quantum simulations were performed for circuits up to 25 qubits using the Qiskit Aer simulator, balancing accuracy and computational feasibility. For larger problem sizes, efficient simulation may require tensor network-based methods or access to real quantum hardware. The quadratic speedup of amplitude amplification remains, but practical implementation is constrained by current hardware and software limitations.

3.3 From Tensor Networks to Quantum Circuits

Tensor networks unify the representation of probabilistic models with quantum state encoding, as probabilistic models can be represented as such 2.3.2, while quantum states - for example matrix product states (MPS) and projected entangled pair states (PEPS) - are inherently represented as tensor networks [22]. Therefore tensor networks provide a unified framework for representing and manipulating probabilistic models, as both probabilistic algorithms (e.g.inference), and quantum algorithms (such as Amplitude amplification) operate on these networks, providing a pathway to quantum-enhanced sampling.

3.3.1 Quantum Circuit Construction

To map a tensor network to a quantum circuit, we need to map the intricate structure, involving connections and dependencies precisely. Slice tensor decomposition 2.4.1 helps us decompose the given network to lower-rank tensors (1 and 2, i.e. vectors and matrices representing state vectors and density operators), that can be mapped to quantum states and operations easily. Thus each tensor (i.e. slice) can be encoded as a quantum state and/or a set of parameterized quantum gates. The contraction of tensors, which in the classical setting corresponds to summing over shared indices, is implemented in the quantum setting by entangling qubits or applying multi-qubit gates. For example, in a network where each variable X_i is binary, a qubit is allocated for each variable, and the entries of the tensor slices determine the amplitudes of basis states, which can be applied as parameterized gate-sets.

Operational Steps:
Decomposition
The joint probability tensor $\mathcal{T}[X_1, \ldots, X_n]$ for an n-variable exponential family distribution can be factorized as per 2.4.1:

$$\mathcal{T}[X_1, \ldots, X_n] = \sum_{k=1}^{r} \lambda_k \, \mathcal{A}_k[X_1] \otimes \mathcal{B}_k[X_2, \ldots, X_n]$$

or, more generally, as per 2.4.2:

$$\mathcal{T}[X_1, \ldots, X_n] = \sum_{k=1}^{r} \mathcal{S}_k[X_1] \cdot \mathcal{U}_k[X_2] \cdots \mathcal{V}_k[X_n]$$

where we have the tensor network uniqely decomposed into slices, ready to be represented as quantum states.

This decomposition—closely related to the canonical polyadic (CP) decomposition, it maps naturally to quantum resources: each vector or rank-1 slice defines amplitude weights for a subset of qubits, and higher-order correlations are encoded as entanglement patterns or controlled gates.

Implementation Integrating the above with the earlier sections, the practical quantum circuit mapping unfolds as:

- **State Preparation** $\mathcal{A}$:
  - Prepare the quantum register in a reference state (e.g., $|0\rangle^{\otimes n}$).
  - Apply Hadamard gates to all variable qubits, creating a uniform superposition over all 2^n states.
  - Use CNOT, Toffoli, and (optionally) parameterized rotation gates to encode the logical structure specified by the tensor network slices, projecting immeadiate nodes/results to designated ancilla qubits.
- **Oracle Construction** (O_ϕ):
  - Construct an oracle that flips the phase of those basis states corresponding to solutions (the "good" states satisfying ϕ of the exponential family).
  - In practice, for logical connectives, this can be realized by targeted Z, X, or multi-controlled Z gates operating on the ancilla qubit(s) where the satisfaction of ϕ has been projected.
- **Diffusion Operator** D:
  - Apply the diffusion operator which inverts the state about the mean. This is constructed as applying $\mathcal{A}^{-1}$ (or $\mathcal{A}^{+}$), a phase flip on $|0\rangle^{\otimes n}$, and $\mathcal{A}$ again. Thus $D \propto \mathcal{A}^{-1} MC\hat{Z}\mathcal{A}$

  - Both $\mathcal{A}$ and its inverse are efficient to implement due to the decomposition structure, mirroring the original tensor slice encoding.

- **Amplitude Amplification**:
  - Iteratively apply $Q = DO_\phi$ to amplify the amplitude of the "good" state subspace.
  - The number of iterations k is chosen according to the initial probability and the target amplification, as detailed in Section 3.2.3.
- **Measurement:**
  - Measure the final state in the computational basis.
  - Measure the variable qubits (i.e. the nodes of our tensor network) in the computational basis.

By combining the slice decomposition approach (Section 2.4.1) with tensor-to-circuit compilation presented in this section, this quantum circuit implementation provides a systematic bridge from classical probabilistic and logical models to quantum-enhanced sampling routines. Each step - from state preparation using decomposed tensor slices, to phase-marked oracles, to efficient inversion about the mean—follows directly from the underlying structure revealed by the slice tensor decomposition. This guarantees scalability and resource efficiency for a wide range of complex probabilistic models.

Therefore utilizing the slice tensor decomposition we can map the example Bernoulli distribution to a quantum circuit easily. Each slice being jointly independent would mean that, we can not only encode them one-by-one, we do not even need to consider entangling gates/procedures. So for the distribution:

$$P(x_1, x_2, \ldots, x_n) = \prod_{i=1}^{n} p_i^{x_i}(1-p_i)^{1-x_i}$$

we can encode each slice $p_i^{x_i}(1-p_i)^{1-x_i}$ to a quantum circuit via a sequence of gates, such as:

- Generate a register for each variable, 1 for each slice.
- Apply Hadamard gate $\hat{\mathbf{H}}$ to create superposition.
- Apply rotation gate around the X or Y axes ($\hat{\mathbf{R}}_X$ or $\hat{\mathbf{R}}_Y$) to encode the probabilities of the distribution resulting in 1 or 0, in the amplitude of the quantum state, i.e. mirroring the state resulting in $|1\rangle$ or $|0\rangle$ upon measurement.

Thus when we measure the circuit it should obtain one of the states representing the result of the measurement ($|1\rangle$ or $|0\rangle$), each with a probability that represents the distribution itself, obtained through the amplitude of the state. Also with a rotation applied to a superposition the state remains pure, so the probabilities will sum up to one.
The amplitude amplification can be done for each slice via an easily applicable oracle and diffusion operator:

- as we are working around binary variables a single $\hat{\mathbf{Z}}$ or $\hat{\mathbf{X}}\hat{\mathbf{Z}}\hat{\mathbf{X}}$ gate(set) would suffice to mark the $|1\rangle$ and $|0\rangle$ states respectively,
- the diffusion opreator should consist of the inverse state preparation unitary $\mathcal{A}^{-1}$, and a single $\hat{\mathbf{X}}$ gate to rotate around the mean amplitude of our starting state (esentially flipping $|0\rangle$ to $|1\rangle$).
- Finally $\mathcal{A} \propto \hat{\mathbf{H}}\hat{\mathbf{R}}_X$ could be applied again on all variable qubits, and we will get an amplified probability of obtaining $|0\rangle$ or $|1\rangle$ (depending on the Oracle).

3.3.2 Resource Estimates

The quantum circuit depth and resource requirements depend on the structure and rank of the underlying tensor network:

- **Qubit Count**: Each variable in the model typically requires one qubit for binary variables (or $\lceil \log_2 d_i \rceil$ qubits for d_i-ary variables) as well as one auxiliary qubit (i.e. ancilla qubit) for connecting the cliques of probabilistic model representations 2.3.2.
- **Gate Complexity**: The number of gates scales with the number of tensor slices and the connectivity of the network. For a CP decomposition of rank r over n variables, the circuit requires $\mathcal{O}(rn)$ parameterized gates [23].
- **Circuit Depth**: For chain-like (MPS) or tree-like (TTN) tensor networks, the depth is $\mathcal{O}(n)$ or $\mathcal{O}(\log n)$, respectively.

As we have seen in the example mapping above we did:

- require 1 qubit for each binary variable ($X_k \in \{X_1, X_2, \ldots, X_n\}$),
- as well as 1 Hadamard and 1 rotation gate for the probability encodings. So the state preparation can be done with $\mathcal{O}(2n)$ gates, where n is the number of variables.

- Additionally each slice requires a constant number of gates for the amplitude amplification procedure, which then for k rounds is $\approx \mathcal{O}(k \cdot 2n)$.
- Thus for N variables, the whole procedure results in a depth of $\approx \mathcal{O}(kn)$. Therefore the number of gates scale with the number of tensor slices. In the case of the example (with joint independence between the variables) it does scale linearly. The linear scaling of the state preparation matches the classical state preparation algorithms [24]. The $\mathcal{O}(k)$ scaling of the sampling algorithm on the other hand is quadratically faster than the classical counterparts.

We can see that the mapping is particularly efficient when the tensor network has low rank or sparse structure, as is often the case for models with strong conditional independence. In such scenarios, the number of required gates and the circuit depth can be kept polynomial in the number of variables, making the approach feasible for near-term quantum devices [25].

In summary, the mapping from exponential family distributions to tensor networks, and subsequently to quantum circuits, enables scalable quantum sampling for complex probabilistic models, as seen by the application of amplitude amplification later on. This approach exploits both the structure of the underlying model and the computational power of quantum devices, providing a pathway to quantum advantage in probabilistic inference and machine learning.

Chapter 4

Experimental Evaluation

Our goal in this section is to show the feasibility of the quantum sampling procedure promoted in the previous sections. It should be done by working through a dummy knowledge base, one chosen from the used instances in AI, previously collected in sect. 2.1. After chosing a suitable subject it will be represented as an exponential family, over which slice tensor decomposition will be utilized, so that the now sliced knowledge base can be mapped to a quantum circuit. Each variable will therefore be represented as a qubit, with the logical connections as quantum gates, within each slice, iteratively building the dummy knowledge base, which is the logical formula. Then the sampling procedure will be tested, with the amplitude amplification involved. We will check the probabilities before and after sampling, to see how the *target* state probabilities have been amplified. After this, it should clearly be visible that a quantum enhanced sampling procedure can be utilized on classical knowledge bases, through a robust decomposition and mapping formalism.

4.1 Use Case: Logical Connective Sampling

A logical formula is the representative knowledge base for testing the quantum sampling procedure. It has been chosen as the suitable subject for testing, as we have been working around the **TNReason** module of sampling for neuro-symbolic AI, which predominantly utilizes logical formulas as knowledge bases. This way we will not only test the quantum sampling procedure, but also see if it is implementable to the module we are working in. And if our experimental findings agree with the theory, it will be implemented as a baseline for future quantum samplers, and possibly be utilized around financial datasets.

4.1.1 Problem Setup

The problem is defined as follows: given a logical formula $\mathbf{F}$ (n Boolean variables connected by propositional logical connectives), our goal is to sample satisfying assignments (*target* states) from the exponentially large space of all 2^n possible assignments. For concreteness, let us focus on a n-qubit system encoding a logical connective such as seen in the previous example 2.1, which for the sake of the example will be 6 variables (mapped to qubits), with 19 connectives, each represented as an ancilla qubit. Therefore the whole quantum circuit requires 25 qubits. The set of *target* states, $\mathcal{G}$, consists of all assignments that satisfy the formula. The initial probability of selecting a good state from the uniform distribution is $P_g = M/N = |\mathcal{G}|/2^n$. In the case of the example shown it equals $P_g = M/N = 1/2^6$, as we have $M = 1$ good state, making that our *target*. Our aim is to amplify P_g to near-unity using quantum amplitude amplification.

4.1.2 Exponential family representation of the Logical Formula

The logical formula $\mathbf{F}$ can be encoded as an exponential family distribution as per 2.5:

$$p(x) = \exp\{\langle\theta, \phi(x)\rangle - A(\theta)\}$$

Serving as the sufficient statistics for the exponential family is $\hat{\mathbb{1}}[\mathbf{F}]$, the indicator function for the formula. θ is the (unnormalized) vector of the canonical parameters, showing the effect of the sufficient statistics as it has been deduced in sect. 2.2.1. This value for θ in our case is:

$$\theta = \begin{pmatrix}\theta_g \\ \theta_b\end{pmatrix}$$

which for θ_g and θ_b is:

- zero, whenever the indicator function gives a result of 'FALSE'/0
- ∞, whenever it is 'TRUE'/1

Using this representation, θ can be understood as the weight of the truth value of the formulas, coming directly from the sufficient statistics being the indicator function of the logical formula. The log-partition function '$\exp(-A(\theta))$' can be rewritten with Z, serving as the normalization constant.
Thus the exponential family is

$$p(x) = \frac{1}{Z}\exp\left\{\theta \cdot \hat{\mathbb{1}}[\mathbf{F}]\right\} \tag{4.1}$$

Using this representation of the indicator function and canonical parameters as weights, we get probabilities:

- $p(x = 1) = \frac{Me^{\theta_g}}{(N-M)e^{\theta_b}+Me^{\theta_g}} = P_g$
- $p(x = 0) = \frac{(N-M)e^{\theta_b}}{(N-M)e^{\theta_b}+Me^{\theta_g}} = P_b$

with $N = 2^n$ as all the possible states, M of which are *target* states. Being a *target* state means the indicator function resulting in 1! This gives a great starting point for us, as for both the 'good' and 'bad' states, wether $\theta = 0$ this reduces to the uniform distribution; and as $\theta \to \infty$, $P \to 1$ and the distribution concentrates on the satisfying assignments. Thus the expectation is this, that when the logical formula is mapped to a quantum circuit, an uniform distribution of variables is given, where all the outcomes (i.e. final states) have the same probability of $\frac{1}{N}$. And when the probability of the *target* states are amplified, only the canonical parameter of the formula will change, as it will diverge to infinite values ($lim_{\theta\to\infty}(e^{\theta}) = \infty$). The sufficient statistics however, should remain the same, esentially keeping us in the same exponential family with tuned variables, to match our amplified quantum states.
Then we need to apply slice decomposition on the defined exponential family to map each logical connection to the quantum circuit at hand. Following the definition in section 2.4.1 we can slice the logical formula by each connective, thus making it straightforward to iteratively have every detail embedded into our initial state $|\psi\rangle$, prepared by the unitary $\mathcal{A}$, the direct result of the decomposition.

4.1.3 Amplitude Amplification for Exponential Families

When the locical formula is mapped to a quantum circuit, we start from a uniform distribution of variables, and slowly amplify the probability of the *target* states, thus changing the probability of finding such.

Our expectation, and goal to prove, is that only the canonical parameter of the formula will change, whilst the sufficient statistics should remain the same. As when the amplitude of the *target* states are amplified, the probabilities are magnified. Thus as per the definition for the exponential family in eq. 4.1, θ_g will diverge to infinite values. This way the procedure is esentially keeping us in the same exponential family with finely tuned variables, to match the amplified quantum states.

Mathematically, if the initial probability of a good state is P_g^0, then after k applications of amplitude amplification, the probability becomes $P_g^k = \sin^2\left((2k+1)\frac{\alpha}{2}\right)$, where $\frac{\alpha}{2} = \arcsin(\sqrt{P_g^0})$, is the angle of the state in H_ψ. In exponential family terms, this corresponds to a shift in the canonical parameter:

$$\theta_g^k = \ln\left(\frac{(1-P_g^0)P_g^k}{P_g^0(1-P_g^k)}\right) \tag{4.2}$$

which can be rewritten as:

$$\theta_g^k = \ln\left(\frac{P_g^k}{1-P_g^k}\right) - \ln\left(\frac{P_g^0}{1-P_g^0}\right) \tag{4.3}$$

So the canonical parameter for the *target* states θ_g^k could be obtained as the the difference of log-odds (i.e. *logit*, the inverse of the *sigmoid*) between the current probability P_g^k (the probability after k rounds of amplification), and the initial probability P_g^0.

This provides a direct link between quantum amplitude amplification and classical parameter updates in probabilistic models.

4.1.4 Quantum Circuit Implementation

The mapping from an exponential family model to a quantum circuit uses the slice decomposition of its tensor network representation. This operational workflow links the mathematical structure of probabilistic graphical models directly to the physical implementation of quantum sampling algorithms. The explicit role of slice tensor decomposition is to enable a direct, scalable quantum encoding of the high-dimensional probability distribution, efficiently reflecting its conditional independence structure and logical symmetries.

In this section, I am illustrating how a specific logical formula is mapped to a quantum circuit using the slice tensor decomposition of its exponential family representation.

Given a logical formula $\mathbf{F}$ first defined in sect 4.1.1, and represented as an exponential family distribution in sect. 4.1.2:

$$p(x) = \frac{1}{Z} \exp\left\{\theta \cdot \hat{\mathbb{1}}[\mathbf{F}]\right\}$$

where, just like in eq. 4.1, $\hat{\mathbb{1}}[\mathbf{F}]$ is the indicator function for the formula $\mathbf{F}$ - i.e. the sufficient statistics of the exponential family, whilst θ is the canonical parameter, and Z is the normalization constant.

To map this to a quantum circuit, we are following the previously outlined construction and amplification schemes from sect. 3.3.1:

1. **Slice Tensor Decomposition**: The indicator function $\hat{\mathbb{1}}[\mathbf{F}]$ naturally partitions the joint tensor representing the distribution into two slices—one for satisfying ("good") and one for non-satisfying ("bad") assignments. Mathematically, the joint distribution tensor is decomposed as:

$$T[x] = \theta_g \cdot \hat{\mathbb{1}}[\mathbf{F} = 1] + \theta_b \cdot \hat{\mathbb{1}}[\mathbf{F} = 0]$$

   where the coefficients of the canonical parameter vector reflect the weights in the exponential family, as defined in sect. 4.1.2. Both θ_g and θ_b start off as 0, thus for the probabilities we have:

$$p(x=1) = \frac{Me^{\theta_g}}{(N-M)e^{\theta_b} + Me^{\theta_g}} = P_g = \frac{M}{N}$$
$$p(x=0) = \frac{(N-M)e^{\theta_b}}{(N-M)e^{\theta_b} + Me^{\theta_g}} = P_b = \frac{N-M}{N}$$

As with the logical formula mapped mapped as a quantum state, we should have an uniform superposition of variables, i.e. equal probabilities for all N states, $P_i = \frac{1}{N}$.

2. **Quantum State Preparation**: The logical formula is compiled into a quantum circuit using ancilla qubits. Apply Hadamard gates to all variable qubits to create a uniform superposition over all 2^n possible inputs, then use Toffoli and controlled gates to compute the value of $F(x)$ onto an final ancilla qubit. This then represents the whole formula, so it will be called the *indicator qubit.*

3. **Oracle Marking**: A Z gate (phase flip) is applied to the ancilla qubit, conditionally marking the satisfying assignments. This realizes the "slice selection" from the tensor decomposition within the quantum circuit.

4. **Diffusion and Amplitude Amplification**: The standard amplitude amplification procedure is then applied, increasing the probability amplitude on the "good" slice. After the desired number of amplification rounds, measurement yields satisfying assignments with high probability, while the underlying tensor slice structure ensures the exponential family is preserved with an updated parameter θ.

The pseudocodes for the test example can be seen in the Appendix A. In summary, this process implements the slice decomposition of the exponential family for a logical formula as a natural quantum circuit: logical structure—encoded as tensor slices—is mapped onto programmable quantum operations and oracles, efficiently targeting the satisfying assignments for sampling and inference.

4.2 Results and Analysis

After k rounds of amplitude amplification, the probability of measuring a good state increases from P_g^0 to $P_g^k = \sin^2((2k+1)\alpha)$. Deduced from the starting probability for a *target* state, $\alpha = \arcsin(\sqrt{P_g^0})$. The canonical parameter of the exponential family updates as seen in eq 4.3.

The changes in probabilities of the given logical formula can be seen in the following figures:

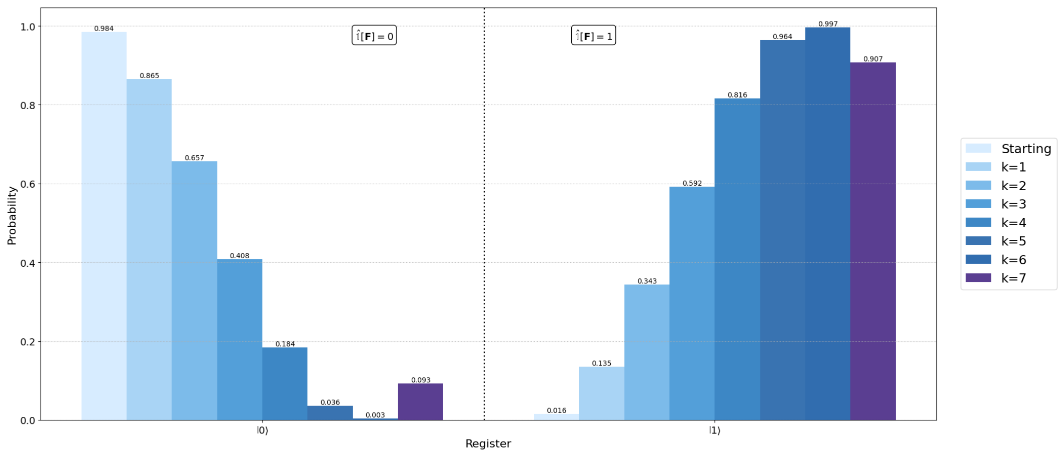

(a) Probability P_g of measuring TRUE/FALSE value on the logical formula, indicated by the value of the *indicator qubit*

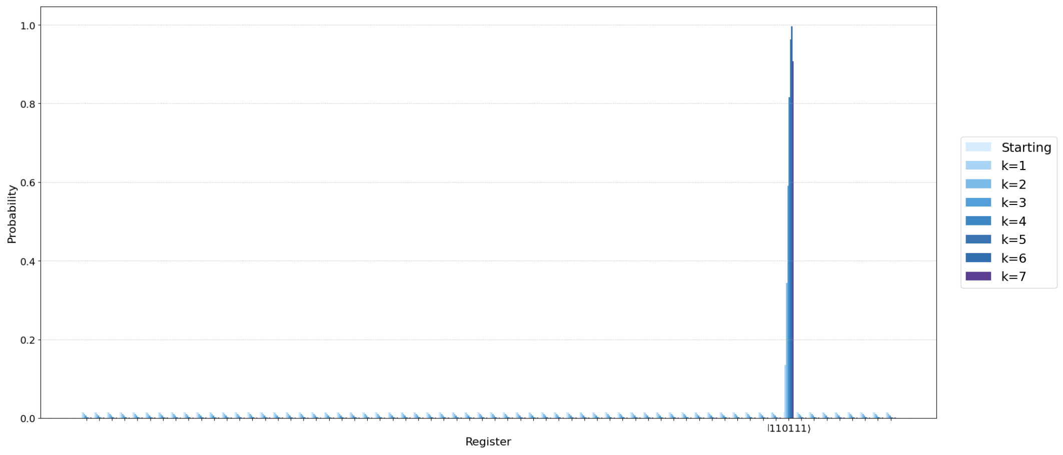

(b) Probabilities of the variable qubit values. The *target* state is visible, it will result in the value of the *indicator qubit* being 1

Figure 4.1: Changing *indicator qubit* and variable qubit state probabilities after k iterations of Grover rotations on a given logical formula $\mathbf{F}$.

We can see that we have achieved near perfect amplification after 6 steps, which is in agreement with the theory presented in sect. 3.2.3, that $k = \lfloor \frac{\pi}{4}\sqrt{\frac{1}{P_g}} \rfloor = \lfloor \frac{\pi}{4}\sqrt{\frac{64}{1}} \rfloor = 6$. The seventh step, as expected, lowers the success probability, meaning that we have overrotated. This overrotation in on par with our calculations for the graphical interpretation of the parameters in sect. 3.2.3.

The corresponding changes angle, probabilities and θ_k are:

Iteration (k)	P_g	α_k (rad)	θ_k
0	0.016	0.126	0
1	0.134	0.375	1.543
2	0.344	0.626	2.763
3	0.592	0.878	3.781
4	0.817	1.129	4.905
5	0.963	1.378	6.668
6	0.997	1.516	9.215
7	0.908	1.263	5.698

Table 4.1: Amplification of probability and exponential family parameter over iterations.

Interpretation: The amplitude amplification procedure efficiently concentrates probability mass on the set of satisfying assignments. This was achieved under $\mathcal{O}(k)$ steps, preserving quadratic speedup over classical sampling methods. The other important result is that the process preserves the exponential family structure of the distribution, with the canonical parameter θ evolving according to the amplification dynamics shown in eq. 4.3. This demonstrates the compatibility of quantum amplitude amplification with classical probabilistic modeling frameworks, showing the viability of the sampling approach.

4.2.1 Canonical Parameter Dynamics in Large-Scale Simulations

While the initial example demonstrated precise amplification behavior for a relatively small quantum circuit - comprising 6 variable qubits and 19 ancillary qubits; the following figures (4.2 and 4.3) do not stem from direct simulation of a larger circuit as with current hardware, classical simulation is intractable, while consumer grade trapped-ion computers are not available for this large qubit numbers. Rather, they illustrate the theoretically calculated dynamics of the angle, probability, and canonical parameters, extended to the regime of much smaller *target* state probabilities and therefore a greater number of amplitude amplification rotations. This approach reinforces the generality and robustness of the theoretical models presented earlier, and allows for a clearer depiction of amplitude dynamics and the evolution of exponential family parameters under deep amplification sequences.

Sinusoidal Variation of Sampling Probabilities As we have seen previously in eq. 4.3, the core mechanism underpinning amplitude amplification is a rotation in the two-dimensional subspace of the state space - spanned by the "good" states (those satisfying the desired logical formula) and the "bad" states (non-satisfying). The probability of measuring a "good" state after k iterations is given by

$$P_g^k = \sin^2\big((2k+1)\frac{\alpha}{2}\big),$$

where $\alpha = \arcsin\sqrt{P_g^0}$ is related to the initial probability of the good states in the uniform superposition.

The sinusoidal waveforms in the figures 4.2 vividly illustrate this fundamental oscillatory behavior: with each application of the amplification operator, the likelihood of observing a target solution state upon measurement is periodically increased. It leads to an optimal number of iterations corresponding to the peak of the sinusoid. Beyond this point, further iterations induce overrotation, causing the probability of success to decrease, as evidenced by the downturn observed in the latter part of the figure.

Canonical Parameter Explosions and Their Interpretation The canonical parameter θ associated with the canonical representation of the exponential family undergoes shifts in close ties with the success probability P_g^k. The relationship ties the probability dynamics to changes in the distribution parameters via

$$\theta_g^k = \ln\left(\frac{P_g^k}{1-P_g^k}\right) - \ln\left(\frac{P_g^0}{1-P_g^0}\right)$$

capturing the evolution of θ as a differential log-odds ratio between the amplified and initial state probabilities.

The sinusoidal behavior of P_g^k translates into a highly non-linear, even discontinuous, evolution of θ_g. Near points where P_g^k approaches unity or zero, the canonical parameter exhibits steep, near-explosive growth, resembling the vertical asymptotes in the log-odds function. This shootout of θ_g effectively tightens the probability mass around the solution set, pushing the distribution towards deterministic support on the satisfying states. The dynamics can be seen in figures 4.2 compared to the sinusoidal change in probability, and in subfigure 4.3a, comparing the θ_g to θ_b.

Such shifts in θ, as being deductable from the probabilities and angles of the *target* state, highlight the capabilities of the procedure. Quantum amplitude amplification increases success probabilities, thus also tunes the parameters of the underlying exponential family representation. In effect, this quantum sampling process updates the distribution's parameters analogous to classical iterative parameter update schemes, yet achieves this transformation quadratically faster in the size of the state space.

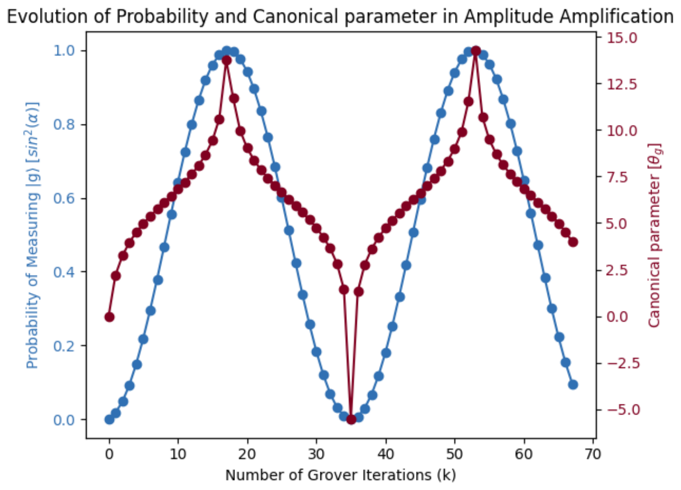

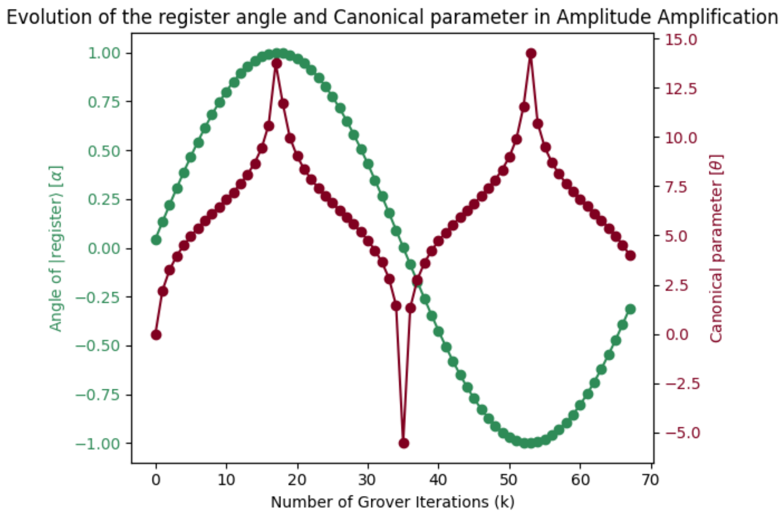

Figure 4.2: **Series of Grover rotations on a given logical formula.** The expected shootout in the canonical parameters of the exponential family can be seen in both figures. First it is compared to the change in probability, secondly against the angle of the register. The log-odds function, with which we define θ_k, has vertical asymptotes at $P = 0$ and $P = 1$, with the added change in behaviour coming from the non-monotonic, but sinusoidal change of P_g^k. This understates those explosive 'jumps', as the function reacts extremely to values close to 0 or 1, which shows that with near perfect amplification, when $P_{\mathcal{G}} \to 1$, we have a local maximum in the canonical parameter.

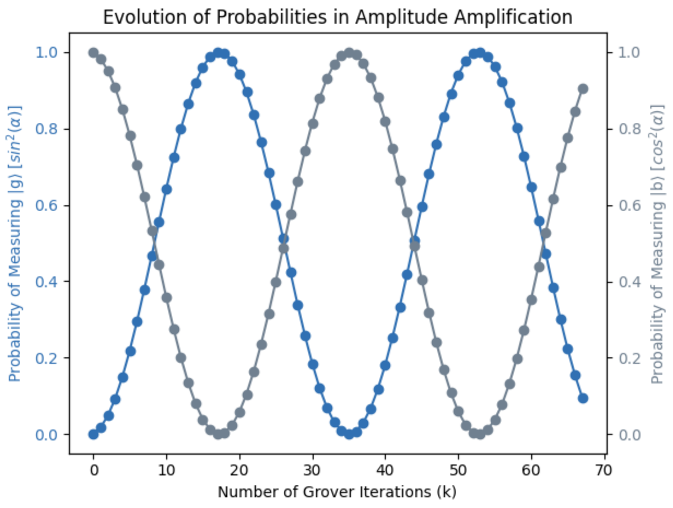

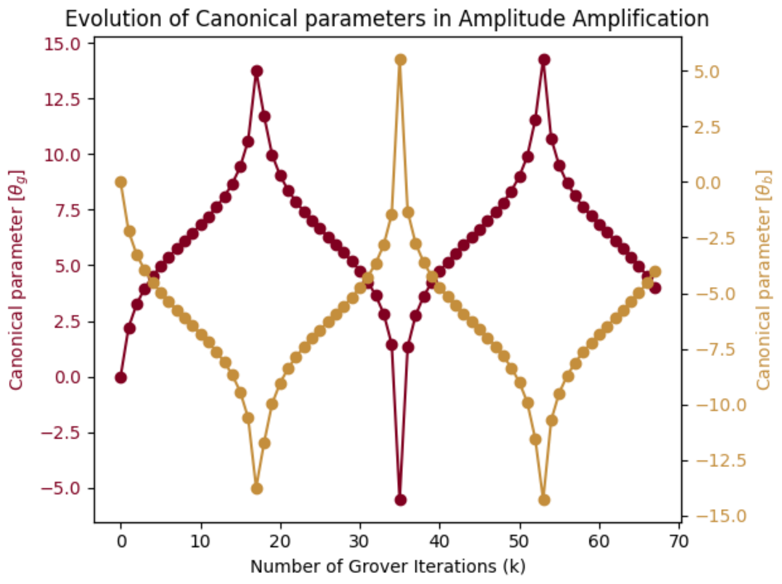

Figure 4.3: **Probabilities and canonical parameters of the** *good* **and** *bad* **states.**t is visible, that while the probability of finding a *target* state, and of not, sums up to one. After each Grover iteration, we will have $P_g^i + P_b^i = 1$. The vector of canonical parameters however is unnormalized, as it is just defining relative weights for outcomes. The normalization is handled by the log-partition function $A(\theta)$. This not only shows us how the parameters of the underlying exponential family representation are tuned, but also serves as a proof, that only the canonical parameter of the formula changed, whilst the sufficient statistics remains the same.

4.3 Generalization and Scalability

These extended theoretical results are consistent with, and importantly reinforce, the findings from the earlier six-qubit system discussed in Section 4.2. In the smaller system, the evolution of $P_g^{(k)}$ and $\theta^{(k)}$ closely matched analytic predictions, with the monotonic increase and subsequent overrotation being clearly visible over a few amplification steps. This close correspondence between simulation and theory provided a solid foundation. The extrapolated dynamics for lower target probabilities and additional amplification rotations further validate the robustness and generality of the theoretical framework, even in regimes beyond those directly simulated.

The repetition of the sinusoidal profile and canonical parameter "explosions" in this setting serves to validate the universality of the amplitude amplification mechanism and its framework via exponential family parameters. It also confirms that the canonical parameterization remains a robust and meaningful descriptor of the distribution throughout the amplification process, regardless of system size. The scalability of these characteristic behaviors confirms that quantum amplitude amplification can serve as an effective primitive within hybrid quantum-classical workflows, feeding back adjusted parameters into classical inference engines. The approach thus generalizes to larger logical connectives and higher-dimensional systems. For n-qubit systems with more complex formulas, the mapping to exponential families and utilizing slice tensor decomposition remains valid, and the quantum circuit construction follows the same principles. Of course real-life scalability is determined by the complexity of the distributions, therefore the circuits, and also the available quantum resources. Nevertheless, having these effects observed in a large-scale simulation offers confidence that hardware developments targeting increased qubit counts and connectivity can harness the modeled phenomena to achieve substantive quantum advantage in AI tasks.

Chapter 5

Benchmarking and Comparative Analysis

After presenting a small test example for the quantum enhanced sampling procedure, where we have seen the feasibility of the algorithm, we need to turn our attention to the speed of the procedure. First it will be checked asymptotically, how it stacks up against classical sampling procedures; then how utilizeable and robust it is on a selected current state NISQ platform.

5.1 Classical Sampling Methods

Sampling is the process of drawing representative instances from a dataset or knowledge base, serving as a fundamental operation in machine learning and artificial intelligence workflows. Classical sampling methods reviewed here include the brute-force enumeration, rejection sampling and Markov Chain Monte Carlo (MCMC) methods, each with distinct strengths and limitations [26].

5.1.1 Brute-Force Enumeration

Brute force sampling, also known as exhaustive enumeration, is the most direct approach to sampling from a probability distribution: it systematically generates and evaluates every possible state in the sample space. For a discrete distribution over N states, this means explicitly listing all N configurations, computing their probabilities, and either selecting samples according to their weights or simply iterating through all possibilities.

While conceptually simple and guaranteed to be exact, brute force methods are only feasible for very small systems. For problems involving n binary variables, the number of all possible states is $N = 2^n$. Thus the cost grows exponentially with n, the time and memory complexity scaling as $\mathcal{O}(2^n)$. This is a classic example of the ‘curse of dimensionality’ or combinatorial explosion.

Brute force enumeration is sometimes used as a baseline for validating other sampling algorithms or for very small models. However, for most real-world applications, the exponential scaling renders brute force approaches intractable. Even modest increases in n quickly make the approach impractical, motivating the use of more sophisticated methods such as rejection sampling, MCMC, or quantum algorithms.

5.1.2 Rejection Sampling

Rejection sampling is a fundamental technique for generating samples from a target distribution $f(x)$ when direct sampling is impractical. The method uses a proposal distribution $g(x)$, from which sampling is easy, and accepts or rejects each candidate based on the ratio $f(x)/(Mg(x))$, where M is a constant such that $M \geq \sup_x p(x)/q(x)$ for all x. The efficiency of rejection sampling heavily depends on the choice of the proposal distribution; if $g(x)$ poorly approximates $f(x)$, the acceptance rate drops and the method becomes computationally inefficient [27]. The coice of said proposal distribution will define the M value, from which a suitable acceptance rate can be deduced. Despite its simplicity, rejection sampling can be wasteful for high-dimensional or rare-event scenarios, as the expected number of trials to obtain one valid sample scales as $\mathcal{O}(M)$. In rare events, where P_g – the probability of a *target* state – is low, matched with a proposal distribution resulting in a high M value $\approx \frac{1}{P_g}$, resulting in a computational complexity of $\mathcal{O}(\frac{1}{P_g})$, which just like with brute-force algorithms, is becoming prohibitive for rare events ($P_g \ll 1$). With an easy-to-sample distribution, or a suitable proposal one, the value for M will be much lower, and the acceptance rate higher. This means in the end a well built rejection sampling can achieve over the previously defined complexity, albeit only by a constant multiplier.

5.1.3 Markov Chain Monte Carlo (MCMC)

MCMC methods, such as the Metropolis-Hastings algorithm and Gibbs sampling, construct a Markov chain whose stationary distribution is the target distribution [28]. By sequentially generating correlated samples, MCMC can explore complex, high-dimensional distributions even when direct sampling or rejection sampling is infeasible. The key advantage of MCMC is its flexibility: it only requires the ability to compute the (unnormalized) density of the target distribution. However, MCMC methods can suffer from slow mixing, especially in multimodal or high-dimensional spaces, and require careful tuning to ensure convergence and independence of samples.
MCMC constructs a Markov chain converging to $p(x)$. For Gibbs sampling, with N being the number of possible states:

- Mixing time scales as $\mathcal{O}(e^N)$ for multimodal distributions
- Per-iteration cost: $\mathcal{O}(N)$ for local updates

- Suffers from slow mixing in high dimensions due to metastability

So while classical sampling methods such as brute-force methods, rejection sampling and MCMC are widely used and well-understood, neither method achieves better than linear scaling in $1/P_g$ or exponential in N, thus they face significant challenges in the context of high-dimensional, structured, or rare-event distributions.

5.2 Quantum vs. Classical: Asymptotic Speedup

Quantum amplitude amplification achieves a quadratic improvement, requiring only $\mathcal{O}(1/\sqrt{P_g^0})$ queries. This has been shown by the calculations in section 3.2.3 and backed up by a dummy example in section 4.2. This follows from Grover's theorem and its generalization to amplitude amplification as defined in sect. 3.2:

Theorem 5.2.1 (Brassard et al. 2000)**.** *Given an initial state $A|0\rangle$ with good-state probability $P_g^0 = \sin^2\alpha$, after $k = \lfloor \frac{\pi}{4}\sqrt{\frac{1}{P_g^0}} \rfloor$ iterations of $\mathbf{Q} = -\mathcal{A}\mathbf{S}_0\mathcal{A}^{-1}\mathbf{S}_\chi$, the probability of measuring a good state satisfies:*

$$P_g^k = \sin^2((2k+1)\alpha) \geq 1 - P_g^0 = P_b^0 \tag{5.1}$$

Proof. The state evolution under Q performs a rotation in a 2D subspace spanned by $|\psi_g\rangle$ and $|\psi_b\rangle$ 3.2.3. After k iterations:

$$Q^k A|0\rangle = \sin((2k+1)\alpha)|\psi_g\rangle + \cos((2k+1)\alpha)|\psi_b\rangle$$

Choosing $k = \lfloor \frac{\pi}{4}\sqrt{\frac{1}{P_g^0}} \rfloor$ yields $(2k+1)\alpha \in [\pi/2 - \alpha, \pi/2 + \alpha]$, giving $P_g^k \geq \cos^2\alpha = 1 - P_g^0 = P_b^0$. Thus after k iterations we have a probability P_g^k higher than P_b^0. □

This demonstrates that $\mathcal{O}(1/\sqrt{P_g^0})$ iterations suffice to amplify the success probability near 1, quadratically faster than classical sampling methods.

5.2.1 Full Circuit Depth Analysis

Although we see that the amplitude amplification achieves a quadratic improvement over classical algorithms, it is only the 'search' part of our procedure, and the quantum advantage must account for full circuit depth, not just oracle queries. Thus we need to include the state preparation unitaries as well:

- D_A: Depth of state preparation circuit
- D_O: Depth of oracle implementation

- D_D: Depth of diffusion operator

The total depth for k iterations is:

$$D_{\text{total}} = D_A + k(D_O + D_D) \tag{5.2}$$

Which in my implementation sums up to:

- Uniform preparation: $D_A = \mathcal{O}(n) \to$ Hadamard gates on all qubits are $\mathcal{O}(1)$ with utilizing paralellism plus NOT/Toffoli gates for logical formula mapping are $\mathcal{O}(cn)$
- Logical oracle: $D_O = \mathcal{O}(1) \to$ as only a single $\hat{Z}$ gate is applied on the *indicator qubit* (as it represents the whole logical formula).
- Diffusion: $D_D = \mathcal{O}(2n)$ (essentially overlapping with the state preparation unitary)

Thus the total depth of the circuit comes down to:

$$D_{\text{total}} = \mathcal{O}(n + k(2n+1))$$

which equals for $k \approx 1/\sqrt{P_g^0} = \sqrt{2^n} = 2^{n/2}$

$$D_{\text{total}} = \mathcal{O}(n + 2^{n/2}(n+1))$$
$$D_{\text{total}} \approx \mathcal{O}(n \cdot 2^{n/2})$$

The quantum method gives a quadratic (square-root) speedup asymptotically when put up against the classical sampling methods listed in sect. 5.1.

5.3 Resource Estimation and Practical Feasibility

The choice of quantum hardware platform is a critical factor in translating theoretical quantum speedup into practical, real-world performance. Different technologies offer distinct trade-offs in terms of gate speed, fidelity, connectivity, and scalability. These properties directly affect the feasibility and efficiency of implementing quantum algorithms, such as the proposed sampling procedure.

5.3.1 Platform proposal

The selection of a quantum hardware platform should be guided by the specific requirements of the task at hand. For this thesis, the focus is on sampling from complex logical connectives and exponential family distributions with utilizing amplitude amplification, i.e. repeated Grover's algorithm. When evaluating platforms for such algorithms that require deep circuits and many multi-qubit entangling gates, key considerations include:

- **Gate Fidelity and Error Rates:** High-fidelity gates are essential to maintain coherence and ensure the reliability of sampling results, especially as circuit depth increases.
- **Coherence Times:** Longer coherence times allow for more complex algorithms to run without significant decoherence, which is crucial for amplitude amplification and other iterative procedures.
- **Qubit Connectivity:** All-to-all connectivity enables direct entanglement between any pair of qubits, reducing the need for SWAP gates and simplifying circuit compilation for highly non-local operations.
- **Native Gate Set:** The availability of native multi-qubit gates or efficient decomposition of logical operations can greatly affect the overall circuit depth and execution time.
- **Scalability:** The ability to scale up to larger numbers of qubits without a significant drop in performance is important for tackling high-dimensional sampling problems.

Platform Selection Rationale

While superconducting qubit platforms offer fast gate times and are widely accessible [29], their limited qubit connectivity (nearest neighbour) and shorter coherence times can become bottlenecks for deep or highly connected circuits. In contrast, trapped ion quantum computers [30] provide several compelling advantages for this class of problems:

- **All-to-All Connectivity:** Eliminates the need for SWAP gates, allowing direct implementation of multi-qubit logical connectives and reducing compilation overhead.
- **Superior Gate and Measurement Fidelity:** Minimizes cumulative error, making it feasible to execute longer circuits with high accuracy.
- **Native support for multi-qubit gates:** Some platforms implement multi-qubit entangling gates directly, further reducing circuit depth for logical oracles and diffusion operators.
- **Exceptionally Long Coherence Times:** Supports deep amplitude amplification sequences and complex sampling routines without significant loss of quantum information.
- **Scalability:** Recent advances have demonstrated the ability to operate with dozens of qubits, with roadmaps to even larger systems.

So, although superconducting qubits have been the workhorse of many quantum computing experiments, trapped ion platforms are particularly well-suited for quantum sampling tasks that involve high circuit depth and complex logical structure. For these reasons, it is the platform, which poses as the most well-suited choice for the quantum samplig algorithm. Trapped ion platforms are quite accessible as well, with many instances being provided by individual companies and research groups. The following table details the relevant hardware specifications and performance characteristics of trapped ion quantum computers, providing a concrete foundation for resource estimation and benchmarking of the proposed quantum sampling algorithms.

It is important to emphasize that generic quantum circuits must be transpiled to run efficiently on trapped ion platforms. Transpilation converts a circuit into an equivalent sequence of gates native to the hardware, such as single-qubit GPI/GPI2 gates and multi-qubit Mølmer-Sørensen (MS) gates. In my case, this process has significantly increased the number of gates compared to the original logical gate count - a *constant* factor that was not fully accounted for in the initial resource and turnover time calculations. Nevertheless, the total gate count after transpilation remains comparatively low, primarily due to the intrinsic all-to-all connectivity feature of trapped ion systems, which eliminates the need for costly SWAP gates required on other architectures with limited qubit connectivity. Thus, despite the gate count increase from transpilation, trapped ion platforms maintain a substantial advantage for implementing highly entangled circuits such as those used in amplitude amplification, where alternate platforms would suffer from a heavy overhead due to numerous SWAP operations.

5.3.2 Circuit Compilation and Scaling

For a general n-variable logical formula (with $N = 2^n$ states and one *target* state, $p_g = 1/N = \frac{1}{2^n}$) the depth is:

$$D_{\text{total}} \approx \mathcal{O}(n \cdot 2^{n/2})$$

following our calculations in sect. 5.2.

Transpilation Considerations: Although some logical gates (e.g., Toffoli, multi-controlled $\hat{Z}$) are not native to trapped ion hardware, all-to-all connectivity and high-fidelity two-qubit gates enable efficient transpilation. The absence of SWAPs and the possibility of direct multi-qubit entangling gates (e.g., Mølmer–Sørensen) mean that even transpiled circuits remain shallow compared to superconducting platforms for the same logical depth, even with the previously mentioned gates being native on such platofmrs.

5.3.3 Quantum vs. Classical Runtime Scaling

For a target probability $P_g^0 = 1/2^n$:

- **Classical sampling (brute force or rejection):**

  $$T_{\text{classical}} = \frac{1}{P_g^0} \cdot t_c = 2^n \cdot t_c$$

  where t_c is the classical step time (e.g., 1 ns). Rejection sampling only differs from this with a constant multipier.

- **Quantum amplitude amplification:**

  $$T_{\text{quantum}} = \frac{1}{\sqrt{P_g^0}} \cdot D_{\text{iter}} \cdot t_g = 2^{n/2} \cdot n \cdot t_g$$

  where t_g is the quantum gate time.

5.3.4 Turnover Point Analysis

Quantum advantage is achieved when $T_{\text{quantum}} < T_{\text{classical}}$, or:

$$2^{n/2} \cdot (1 + 2n) \cdot t_g < 2^n \cdot t_c$$

Single qubit gate times are tens of microseconds to about 50 microseconds on average, while two-qubit gates take 50-500 microseconds typically. Thus a crossover point can be approximated on average as:

$$10^5 \cdot (1 + 2n) < 2^{n/2}$$

Numerical solution:

- For $n = 30$: $10^5 \times 61 = 6.1 \times 10^6 < 2^{15} = 32,768$ (not yet quantum-advantaged)
- For $n = 40$: $10^5 \times 81 = 8.1 \times 10^6 < 2^{20} = 1,048,576$ (not yet quantum-advantaged)
- For $n = 50$: $10^5 \times 101 = 1.01 \times 10^7 < 2^{25} = 33,554,432$ (close to quantum advatage)
- For $n = 60$: $10^5 \times 121 = 1.21 \times 10^7 < 2^{30} = 1,073,741,824$ (quantum is much faster)

Conclusion: The quantum-classical turnover for rare-event sampling occurs at $n \approx 50$ qubits on current trapped ion hardware.

5.3.5 Performance on trapped ion hardware

Trapped ion quantum computing exhibits distinctive performance characteristics across several key metrics. Coherence times for trapped ion qubits can reach up to about 60 seconds in the best cases, often spanning several seconds to tens of seconds on average, with worst-case coherence times still substantially longer than those of many other qubit platforms. Single-qubit gate times typically range from around 1 microsecond in optimized setups to tens of microseconds on average, with worst-case times extending into hundreds of microseconds. Two-qubit gate times are generally longer, spanning from approximately 1 microsecond for advanced pulse-controlled gates up to hundreds of microseconds or milliseconds depending on system specifics and operations involved.

Gate fidelities on trapped ion devices are among the highest in quantum computing. Single-qubit gates can achieve fidelities up to 99.9999%, with averages commonly between 99.5% and 99.99%, while worst-case fidelities remain above 99%. Two-qubit gates exhibit best-case fidelities exceeding 99.9%, averages in the 97.5% to 99% range, and worst cases around 95%, with ongoing research pushing these numbers higher.

These performance metrics illustrate the practical advantages and challenges of trapped ion quantum computing, including long coherence times and high-fidelity gates enabling low-error, relatively fast quantum sampling compared to classical methods. However, gate times - especially for two-qubit operations - remain slower than some other qubit technologies.

Performance and feasibility of the test example

The complete algorithm (test example in chapter 4, state preparation and 6 rounds of amplification) includes around 8500 single-qubit gates (`gpi` and `gpi2`) and 1200 two-qubit `ms` gates. Assuming typical trapped ion gate durations of approximately 20 microseconds per single-qubit gate and 200 microseconds per two-qubit gate, the total execution time could be held under a few seconds, a number that comfortably fits within the coherence window of average trapped ion platforms.

In terms of fidelity, single-qubit gates on trapped ion hardware typically achieve fidelities between 99.5% and 99.99%, whereas two-qubit gates range from about 97.5% to 99.9%. Although the large number of gates compounds errors, the overall fidelity is expected to remain within practical limits for near-term quantum experiments.

In conclusion, the algorithm's duration is compatible with the coherence times of trapped ion qubits, and its fidelity lies within acceptable bounds given current hardware capabilities.

5.3.6 Weak points and Possile improvements

To improve practical quantum advantage in sampling on trapped ion hardware, the following strategies could be considered:

- **Two-qubit fidelities:** Single-qubit gates have achieved great fidelity, focusing research and engineering efforts on increasing two-qubit gate fidelity is critical. Their precision is not lacking compared to other quantum hardware, but with our procedure, where numerous two-qubit gates are utilized, their inaccuracy can lead to fidelity issues. Advancements could involve better pulse shaping, error correction codes designed for two-qubit gates, and refined calibration methods tailored for the ion trap environment.
- **Two-qubit gate times:** Concerning the gate times two-qubit gates can be considered slow compared to other platforms, which can cause issues in deep circuits. Advances in pulse engineering, mode shaping could shorten gate times, nevertheless the high coherence times can make up for it in the long run.
- **Coherence times:** Substantially longer than those of many other qubit platforms, nevertheless by leveraging advanced manufacturing, cryogenic cooling, and improved vacuum or shielding technology can further lengthen the trapped ion coherence times.

Summary: Trapped ion quantum hardware provides a compelling platform for quantum-enhanced sampling, particularly for deep circuits and rare-event problems. The combination of all-to-all connectivity, long coherence times, and ultra-high gate fidelities offsets the slower gate speeds compared to superconducting qubits. As a result, quantum advantage for sampling is projected to emerge at $n \geq 50$ qubits for unstructured search, and significantly earlier for structured or highly parallelizable logical connectives. These features make trapped ion systems especially attractive for scalable quantum machine learning and probabilistic inference in the near future.

Chapter 6

Discussion

6.1 Overview: Contributions within Artificial Intelligence

The findings of this thesis open up a possible solution for the growing challenges in modern machine learning and artificial intelligence. As the algorithmic capability increases, so does the computational depth of the tools required for working with high-dimensional, complex data. Sampling problems cut to the core of numerous applications, from Bayesian inference and generative modeling to combinatorial optimization and decision making under uncertainty.

This thesis brings two major contributions to said matter. The first is the theoretical framework developed, combining exponential families and tensor networks, providing a pathway for mapping structured knowledge bases directly onto quantum states and circuits. This mapping to a quantum circuit is not only unified and applicable to knowledge bases used in ML and AI workflows, but also enables quantum procedures on the data. This leads to the other major result of this thesis, a promising new paradigm: quantum-enhanced sampling with amplitude amplification.

The contributions set up experimentation, comparison, and benchmarking of quantum routines not only against classical baselines, but as foundational components for future hybrid workflows in probabilistic AI.

6.2 Scientific Results

The first contribution's result is the unified framework linking classical and quantum domains. It makes use of exponential family distributions and tensor networks as an essential bridge between the domains. Exponential families bring together a wide range of probabilistic models/distributions, such as Bernoulli, Binomial, Gaussian; as well as propositional logical formulas and probabilistic graphical models. These admit to both canonical (θ-parametrized) and mean-parameter (μ-parametrized) dual descriptions.

Slice tensor decomposition serves two roles: enabling classical scalability for inference and learning by compressing or "slicing" high-dimensional distributions into manageable factors, i.e. slices; and providing a baseline for quantum circuit implementation where local structure is mapped to quantum gates or registers. For example, in models with conditional independence, the decomposition reveals which variables/parameters admit efficient, parallel encoding, thus minimizing the need for multi-qubit - and thus error-prone - entangling gates.

A other key result of this thesis is the possibility of a quantum sampling procedure, and the careful quantification of a speedup compared to classical algorithms. While prior research has highlighted the quadratic advantage for amplitude amplification, this work pushes further, showing an application for the procedure and highlighting how and where quantum algorithms can operate more efficiently. The quadratic reduction in sampling cost (from $\mathcal{O}(1/P_g^0)$ to $\mathcal{O}(1/\sqrt{P_g^0})$ for events of probability P_g^0) is confirmed for structured examples and extended to general exponential family representations.

Empirical Validation and Scalability

Through implementation of quantum sampling routines on up to about 28 qubits using classical simulators, the thesis provides valuable empirical validation - as the test problem in Chapter 4. Notably, by integrating classical circuit-depth analysis with practical quantum implementation (including full gate counts and state preparation costs), the thesis finds the crossover point between quantum and classical speeds and accuaricies. This depends on problem size and problem structure (i.e. dimension and structure of the knowledge base), as well as hardware overheads. The benchmarking results indicate that quadratic speedups are realized in practice for target-finding problems, and that the expected "turnover point" where quantum methods become faster than classical procedures appears within reach as quantum hardware matures. The observed scaling laws for circuit depth, probability amplification, and resource consumption match theoretical predictions.

For low-dimensional models, possibly with independent variables and high *target* probabilities (just like the dummy example of a joint Bernoulli distribution throughout the thesis), quantum methods are efficient but not necessarily advantageous; the speedup emerges decisively for high-dimensional, and rare-event sampling tasks where brute-force, classical rejection or Markov Chain Monte Carlo (MCMC) approaches are exponential in scaling or poorly mixing.

Additionally, the analysis of hardware requirements, like gate fidelities, coherence times, qubit overhead, error rates; offers actionable insights for experimentalists aiming to demonstrate quantum advantage in real-world AI-relevant sampling contexts.

6.3 Implications for quantum enhanced AI

6.3.1 Unifying Symbolic and Probabilistic Reasoning

One of the more subtle implications of this research comes from the fact that logical formulas (e.g., propositional logic, rules, constraints) and probabilistic models (e.g., graphical models, exponential families) can be handled by a unified tensor network formalism. In classical contexts, this enables the growing field of neuro-symbolic AI; melding logical reasoning with probabilistic inference. Quantum computation adds a further layer, allowing these unified models to be encoded, evolved, and measured as quantum states.

This unification is not merely aesthetic. By developing a mathematical framework that represents both logical formulas and probabilistic models as tensor networks, the thesis makes this integration explicit. This common representation enables leveraging tensor decomposition techniques to break down complex knowledge bases - comprised of logical connectives, rules, and probabilistic relationships - into factors that can be handled uniformly. The work bridges a gap between classical AI representations and scalable quantum algorithms it allows for new workflows in knowledge discovery, automated theorem proving, and scientific reasoning where uncertainties are both explicitly modeled and efficiently sampled in ways robust to high-dimensional or combinatorial structure.

6.3.2 Hardware Roadmaps and Near-Term Opportunities

The resource analysis in this thesis suggests that, while current superconducting and trapped ion platforms are still challenged by noise, scalability, and depth, the hardware gap is shrinking. All-to-all connectivity in trapped ion systems, advances in error mitigation, and growing industry roadmaps mean that quadratic quantum speedups for sampling may be demonstrated in prototype tasks within a few years, maybe even for larger systems, with greater depth/number of qubits. Industry leading trapped ion platforms have roadmaps containing 10,000 physical qubits on a single chip, and 99.9%+ two-qubit gate fidelity on development and commercial systems. And this maturing in hardware is due to arrive within a few years [31].

This is especially relevant for domains such as finance, logistics, and scientific simulations, where sampling rare events from highly-structured models is core to risk estimation, optimization, and planning. The methods and mappings detailed in the thesis can be directly transfered to such settings.

6.3.3 The Path to Hybrid Quantum-Classical AI

Another key opportunity is the integration of quantum sampling modules into classical ML/AI workflows. Several computational models and paradigms could be imagined:

- Pre-conditioning classical probabilistic models with quantum-sampled data. As the procedure presented here not only samples the knowledge base but also modifies distribution parameters just like classical iterative parameter update schemes. Thus a bias will be introduced towards *target* states, which preconditions the classical model to easier further sampling.
- Hybrid inference pipelines where challenging components (such as hard constraints or rare events) are delegated to quantum processors, while routine inference remains classical. Or even better, adaptive algorithms, where quantum hardware co-processors are triggered "on demand" when classical samplers fail due to exponential bottlenecks or poor mixing. This depends wether we are sampling from a knowledge base manageable by classical methods, or if quantum takeover is needed. For multivariate distributions certain parts could be handled by classical methods, whilst the harder, classically unfeasible elements should be handed over to an on-demand quantum processing unit.

The TNREASON framework and associated software developed in this research are important steps toward such hybrid modalities. As knowledge bases are represented classically, with logical formulas, or probabilistic graphical models, built in tensor contraction features, and easy to apply classical sampling processes are applicable. Nevertheless with the new paradigm of quanum enhanced sampling involved, we can switch between the two easily, as the same knowledge base representation is utilized, thus it is only a question of preference (and of course computational need).

6.4 Limitations and Open Challenges

Although the proposed algorithm is promising, and with current state hardware maturing real-life tests and utilization is on the boeard, critical evaluation reveals several hurdles from both the theoretical and the practical sides.

Theoretical and Algorithmic Limits

- **Limited to Quadratic Speedup:** Amplitude amplification and Grover-like algorithms do not (in the black-box regime) break the quadratic speedup barrier. For many ML tasks, full exponential speedup remains out of reach, though there is scope for greater than quadratic advantage in structured or oracle-learnable settings.

- **Fast classical algorithms:** Not only quantum algorithms have the opportunity to keep on getting faster. Some modern classical sampling algorithms, such as advanced MCMC variants or variational approaches, may close much of the gap to quantum acceleration - especially for distributions with tractable structure or learnable proposal mechanisms. Thus breaking the quadratic speedup barrier is not only about researching various quantum procedures, but also about making quantum improve faster than the classical algorithms are improving.

- **Real-World Integration:** Even when quantum sampling is theoretically advantageous, real datasets often require extensive data encoding, classical post-processing, and integrated workflow design to ensure that quantum routines genuinely drive end-to-end capability improvement. This problem could be adressed by a more robust decomposition technique, so that classical datasets can fit easier into quantum workflows.

Practical Hardware Bottlenecks

- **Noise and Decoherence:** Even minor gate errors accumulate rapidly in deep circuits. For amplitude amplification, Grover's iteration is applied k times. Therefore the Diffuison operator $\mathbf{D}$ - which is assembled from the state preparation and its inverse - is applied k times, meaning the state preparation unitary are applied $2k$ times. With the vast number of gates, cumulative errors can overwhelm the quadratic speedup, leading to practical constraints on feasible problem sizes in current-state NISQ (Noisy Intermediate-Scale Quantum) devices. Improvements in gate fidelities, or/and in error-correction are needed in the long run, so the number of gates will not be an issue.

- **Oracle complexity:** Of course the amplitude amplification algorithm requires k applications of the Oracle $\mathbf{O}$ as well. For non-trivial logical formulas or multi-level constraints a 'simple' oracle might not suffice as it did here. An efficient phase oracle circuit (that marks the "good" states) is neeeded, although that may require complex ancilla management, multi-controlled Toffoli gates, or large numbers of ancillary qubits. Each adds both gate count and error vulnerability. It could be overcome by automated or semi-automated construction of complex quantum oracles that recognize (or mark) all solutions. For example, with the utilization of an ancillary qubit for the indicator function - just like we have done with the *indicator qubit*, the depth can be greatly reduced.

- **Scalability to Arbitrary Graphs/Models:** Not all classical models decompose compactly or admit efficient tensor network representations. Dense graphical models or highly entangled logical connectives may remain intractable even for quantum routines unless further innovations in model structure, parameterization, or circuit compilation are developed.

6.5 Future Research Directions

Inspired by results and challenges above, exciting paths for continued research include:

- **Development of more expressive and resource-efficient tensor network decompositions.** The slice tensor decomposition utilized in the thesis proved to be useable with both the dummy example and the test knowledge base. As an advancement, the mapping of complex distributions to quantum states and circuits could be more straightforward and robust. This can achieved with numerous tests, where more complex, higher dimensional knowledge bases would undergo the mapping procedure, through slice-decomposing their exponential family representation. Then, a picture can be obtained about the hardships and challanges about mapping highly dependent and intricate structures. This question however is not only about the decomposition itself but the mapping of these structures too, and the representation of structure as quantum operations (gates).
- **Mapped quantum states with a generalized gate set.** To follow up from before, a robust decomposing/mapping algorithm could use a pre-defined set of gates ($\hat{\mathbf{X}}$, $\mathbf{C}\hat{\mathbf{X}}$, $\mathbf{MC}\hat{\mathbf{X}}$) to encode probabilities/amplitudes and dependencies within the knowledge base. The selected gate-set depends on both the structure of the knowledge base, but also the selected quantum platform to be utilizied. With a well defined and carefully selected set, quantum parallelism could be exploited, the gates with the best parameters - such as fidelity, gate-time - could be selected. This way a more precise decomposing and sampling algorithm could be used, that might be able to reach quadratic speedup on smaller systems even. As with amplitude amplification quadratic speedup remains the ceiling of our possibilities, but the turnover point could come sooner, with even less qubits. Another way would be using purely Rotation gates, where we can have precise algorithms on the trapped-ion platforms.
- **Experimental validation on near-term quantum hardware.** A future goal is to generate full-stack benchmarks for both classical and quantum sampling (as hardware matures). Therefore, a clearer picture would be obtained about the speed difference between classical and quantum. With full-stack benchmarks the precision, the robustness and the scalability of the algorithm can be modelled on current state quantum platforms. It would give

a clear picture about the current state of platforms, including runtimes and fidelity, as well as the feasibility of the procedure as of now. Also future platform

- **Investigations into non-standard quantum sampling primitives.** These may surpass quadratic speedup in restricted or adaptive settings (e.g., quantum walks, adiabatic quantum computation, or quantum Boltzmann machines). Higher dimensional sampling issues could be restricted to ancillas, where the amplification would only be made on such final connective qubits, representing the whole distibution.
- **Applications in other domains.** Beyond the example and toy models, direct deployment can be informative in financial data analysis, logistics, computational biology, or AI-driven scientific discovery. It is in order specifically in areas where high-dimensional structured sampling is a limiting factor.

6.6 Conclusions and Outlook

This thesis advances the field by unifying classical representations and quantum implementation of probabilistic and logical models, providing a systematic method for quantum circuit mapping via tensor networks, and empirically verifying quadratic speedups for critical sampling tasks. By quantifying resource demands, identifying the classical to quantum turnover point, and analyzing the role of hardware design, this work builds a bridge between promising quantum theory and future AI applications.

Looking ahead, the role of quantum sampling in AI will likely expand as hardware improves, hybrid paradigms mature, and as real-world bottlenecks in classical probabilistic inference demand fundamentally new computational processes. The duality between logic, probability, tensors, and qubits explored here lays groundwork for a new generation of robust, expressive, and scalable machine learning architectures - where quantum computation is not only an add-on but a core enabler for future artificial intelligence.

Appendix A
Code Listings

Algorithm 1 Logical Expression to Quantum Circuit Mapping

```
function LogicalToQuantum($expression$)    ▷ Automatically maps logical expressions to quantum circuits with dynamic qubit allocation
    $variables \leftarrow$ extract_variables($expression$)
    $num\_ancilla \leftarrow$ count_connectives($expression$)
    $var\_list \leftarrow$ sorted list of $variables$
    $qubits\_map \leftarrow \{$ assign index for each $var \in var\_list\}$
    $ancilla\_start \leftarrow$ length of $qubits\_map$
    $ancilla\_map \leftarrow \{\text{'anc'}_{i+1} : ancilla\_start + i \mid i = 0, \ldots, num\_ancilla - 1\}$
    Update $qubits\_map$ with $ancilla\_map$
    $circuit \leftarrow$ new QuantumCircuit()
    for each $name$ in sorted $variables$ do
        $qreg \leftarrow$ QuantumRegister(1, name=$name$)
        Add $qreg$ to $circuit$
    end for
    $anc\_reg \leftarrow$ QuantumRegister($num\_ancilla$, name="anc")
    Add $anc\_reg$ to $circuit$
    $basis\_qubits \leftarrow$ indices of logical $variables$
    for each $q$ in $basis\_qubits$ do
        Apply Hadamard gate to qubit $q$ in $circuit$
    end for
    $ancilla\_counter \leftarrow [0]$    ▷ mutable counter
    $final\_result \leftarrow$ resolve_expression($expression$, $circuit$, $qubits\_map$, $ancilla\_start$, $ancilla\_counter$)
    return $circuit, qubits\_map$
end function
```

This algorithm takes a logical expression as input and automatically maps it onto a quantum circuit.

It first extracts all the logical variables and counts the number of logical connectives to determine how many ancillary qubits will be needed. It then assigns indices to the variables and ancilla qubits, creating a map for qubit allocation. The quantum circuit is built dynamically with one quantum register per variable and an additional register for the ancilla qubits. The dynamic allocation not only makes it robust, but when going through the circuit we can easily check if the qubits and gates have been applied precisely, by following the names of variables and allocated qubits.

For the state preparation Hadamard gates are applied to all basis qubits to create superposition states. Finally, the expression is recursively resolved into quantum gates through the *resolve_expression* function 2, producing a quantum circuit that represents the whole logical function.

Algorithm 2 Resolve Logical Expression to Quantum Gates

```
function ResolveExpression($expr, circuit, qubits\_map, ancilla\_start, ancilla\_counter$)
▷ Recursively resolve nested logical expressions into quantum gates
    if $expr$ is a variable (string) then
        return $qubits\_map[expr]$
    end if
    if $expr$ is a list with length $> 1$ then
        $gate \leftarrow expr[0]$                                    ▷ Logical connective
        $args \leftarrow expr[1:]$
        $resolved\_args \leftarrow \emptyset$
        $target \leftarrow ancilla\_start + ancilla\_counter[0]$
        Increment $ancilla\_counter[0]$ by 1
        if $gate =$ "not" and length of $resolved\_args = 1$ then
            Apply not gateset on $resolved\_args[0]$ to $target$
        else if $gate =$ "and" and length of $resolved\_args = 2$ then
            Apply and gateset on $resolved\_args[0]$ to $target$
        else if $gate =$ "or" and length of $resolved\_args = 2$ then
            Apply or gateset from $resolved\_args[0]$ to $target$
        else if $gate =$ "xor" and length of $resolved\_args = 2$ then
            Apply xor gateset from $resolved\_args[0]$ to $target$
        else if $gate =$ "implication" and length of $resolved\_args = 2$ then
            Apply implication gateset on $resolved\_args[0]$
        else if $gate =$ "bijection" and length of $resolved\_args = 2$ then
            Apply bijection gateset from $resolved\_args[0]$ to $target$
        else
            Raise an error: Unknown or improperly formatted gate
        end if
        return $target$
    end if
end function
```

This algorithm recursively translates a nested logical expression into corresponding quantum gates within a quantum circuit. It handles base cases where the expression is a simple variable by returning its mapped qubit index. For compound expressions, connectives represented as lists, it identifies the logical connective (such as 'not', 'and', 'or' etc.) and recursively resolves each argument. Ancillary qubits are dynamically allocated to store intermediate results, ensuring no qubit position conflicts. Based on the logical connective, the algorithm applies the appropriate quantum gate operations to the resolved argument qubits and ancilla, effectively constructing the quantum circuit equivalent of the logical formula. If an unknown or malformed gate is encountered, the algorithm raises an error, maintaining robustness. This process enables systematic conversion from classical logic expressions to quantum gate implementations.

Algorithm 3 Oracle Construction

```
function ORACLE1($input\_circ$)
    $n \leftarrow input\_circ$.num_qubits
    $b1 \leftarrow$ Quantum circuit on $n$ qubits
    Apply $Z$ gate to $b1$ on qubit $(n-1)$
    return $b1$
end function
```

For our case a simple Z gate on the final ancilla qubit - the *indicator qubit* - is enough to ‘mark’ the *target* state. This construction for the circuit, where the indicator function is represented as the *indicator qubit* helps us to perform less complex oracles, as the *target* states are those that give 1 for the indicator function - i.e. the *indicator qubit* is in state $|1\rangle$.

Algorithm 4 Quantum Diffusion Operator Construction

```
function DIFFUSION($input\_circ$)
    $n \leftarrow input\_circ$.num_qubits
    $b1 \leftarrow$ Quantum circuit on $n$ qubits
    $b2 \leftarrow b1$ composed with $input\_circ^{-1}$
    for $qubit$ in $0, 1, \ldots, n-1$ do
        Apply $X$ to $b2$ on $qubit$
    end for
    Apply $H$ to $b2$ on qubit $(n-1)$
    Apply $MCX$ (multi-controlled X) to $b2$ controlled by qubits 0 to $n-2$, targeting qubit $n-1$
    Apply $H$ to $b2$ on qubit $(n-1)$
    for $qubit$ in $0, 1, \ldots, n-1$ do
        Apply $X$ to $b2$ on $qubit$
    end for
    $diffusion \leftarrow b2$ composed with $input\_circ$
    return $diffusion$
end function
```

The diffusion operator is constructed from the state preparation unitary $\mathcal{A}$. As it is constructed from a sequence of unitary gates, it itself is unitary and thus reversible. The diffusion operator therefore follows the paragrph and the equation 3.2.2, being assembled from the inverse of the state preparation unitary, a rotation around the mean amplitude of all possible n-qubit states, then the preparation unitary again. Thus this implementation is robust for any state preparation unitary and number of qubits.

Algorithm 5 Grover Iterations with Oracle and Amplifier

```
function ApplyAmplification(circuit, oracle, amplifier)
    rounds ← $k$
    for $i = 1$ to rounds do
        circuit ← circuit composed with oracle composed with amplifier
    end for
    return circuit
end function
```

Finally the Oracle **O** and Diffusion **D** operators are applied in sequence for k number of times. It is according to the calculations in eq. 3.2, as per $k = \lfloor \frac{\pi}{4}\sqrt{\frac{1}{P_g^0}} \rfloor$.

Bibliography

[1] Maximilian Balthasar Mansky et al. *Sampling problems on a Quantum Computer.* Sept. 2023. DOI: 10.1109/qce57702.2023.00062. URL: http://dx.doi.org/10.1109/QCE57702.2023.00062.

[2] Kevin Mallinger Sebastian Raubitzek. *On the Applicability of Quantum Machine Learning.* June 2023. DOI: 10.3390/e25070992. URL: https://pubmed.ncbi.nlm.nih.gov/37509939/.

[3] Stuart Russell and Peter Norvig. *Artificial Intelligence: A Modern Approach, Global Edition.* Pearson, 2021. ISBN: 978-1-292-40113-3.

[4] Rahul Mailcontractor Smita Patil. »Impact of AI and Machine Learning on Financial Services«. In: (2024). DOI: 10.1051/itmconf/20246801021. URL: https://www.researchgate.net/publication/386985798_Impact_of_AI_and_Machine_Learning_on_Financial_Services.

[5] Rachel Gordon. *How AI is improving simulations with smarter sampling techniques.* 2024. URL: https://news.mit.edu/2024/how-ai-improving-simulations-smarter-sampling-techniques-1002.

[6] Artificial Narrow Intelligence ANI. »Sampling techniques«. In: (2021).

[7] Masahiro Suzuki and Yutaka Matsuo. »A survey of multimodal deep generative models«. In: *Advanced Robotics* 36.5–6 (Feb. 2022), pp. 261–278. ISSN: 1568-5535. DOI: 10.1080/01691864.2022.2035253. URL: http://dx.doi.org/10.1080/01691864.2022.2035253.

[8] Ryan LaRose. *A brief history of quantum vs classical computational advantage.* 2024. arXiv: 2412.14703 [quant-ph]. URL: https://arxiv.org/abs/2412.14703.

[9] Blake A. Wilson, Zhaxylyk A. Kudyshev and Kildishev. »Machine learning framework for quantum sampling of highly constrained, continuous optimization problems«. In: *Applied Physics Reviews* 8.4 (Dec. 2021). ISSN: 1931-9401. DOI: 10.1063/5.0060481. URL: http://dx.doi.org/10.1063/5.0060481.

[10] Lov K. Grover. *A fast quantum mechanical algorithm for database search.* 1996. arXiv: quant-ph/9605043 [quant-ph]. URL: https://arxiv.org/abs/quant-ph/9605043.

[11] IQM. »Demonstration of Improved Qubit Quality«. In: *Quantum Computing Report* (2024). URL: https://quantumcomputingreport.com/iqm-demonstrates-continued-improvement-in-qubit-quality/.

[12] Moody's. »Quantum Computing's Six Most Important Trends for 2025«. In: *Moody's Analytics* (2025). URL: https://www.moodys.com/web/en/us/insights/quantum/quantum-computings-six-most-important-trends-for-2025.html.

[13] SpinQ. »Quantum Hardware Challenges«. In: *SpinQ News* (2025). URL: https://www.spinquanta.com/news-detail/quantum-hardware-explained-a-complete-guide.

[14] Number Analytics. *Real-World Applications of Probabilistic Graphical Models.* 2025. URL: https://www.numberanalytics.com/blog/real-world-applications-probabilistic-graphical-models-uncovered-today.

[15] Md Kamruzzaman Sarker et al. »Neuro-symbolic artificial intelligence: Current trends«. In: *AI Communications* 34.3 (2021), pp. 197–209. DOI: 10.3233/AIC-210084. URL: https://journals.sagepub.com/doi/abs/10.3233/AIC-210084.

[16] Vaishak Belle. »On the relevance of logic for AI, and the promise of neuro-symbolic learning«. In: (2024). URL: https://neurosymbolic-ai-journal.com/system/files/nai-paper-792.pdf.

[17] Martin J. Wainwright and Michael I. Jordan. »Graphical Models, Exponential Families, and Variational Inference«. In: *Foundations and Trends® in Machine Learning* 1.1–2 (2008), pp. 1–305. ISSN: 1935-8237. DOI: 10.1561/2200000001. URL: http://dx.doi.org/10.1561/2200000001.

[18] Dan Geiger et al. »Stratified exponential families: Graphical models and model selection«. In: *The Annals of Statistics* 29.2 (2001), pp. 505–529. DOI: 10.1214/aos/1009210550. URL: https://doi.org/10.1214/aos/1009210550.

[19] Michael A. Nielsen and Isaac L. Chuang. *Quantum Computation and Quantum Information: 10th Anniversary Edition.* Cambridge University Press, 2010.

[20] Douglas Youvan. *Beyond the Limit: Implications and Consequences of Violating the No-Communication Theorem.* Dec. 2023. DOI: 10.13140/RG.2.2.16756.32646.

[21] Gilles Brassard et al. *Quantum amplitude amplification and estimation.* 2002. DOI: 10.1090/conm/305/05215. URL: http://dx.doi.org/10.1090/conm/305/05215.

[22] Minzhao L. Aleksandr B. and Atithi A. *Tensor networks for quantum computing.* 2025. arXiv: 2503.08626 [quant-ph]. URL: https://arxiv.org/abs/2503.08626.

[23] Frank L. Hitchcock. »The Expression of a Tensor or a Polyadic as a Sum of Products«. In: *Journal of Mathematics and Physics* 6.1-4 (1927), pp. 164–189. DOI: https://doi.org/10.1002/sapm192761164. URL: https://onlinelibrary.wiley.com/doi/abs/10.1002/sapm192761164.

[24] APXML. *Complexity Theory for Classical and Quantum Algorithms*. Accessed: 2025-08-18. 2025. URL: https://apxml.com/courses/fundamentals-quantum-machine-learning/chapter-1-quantum-ml-foundations-revisited/complexity-theory-classical-quantum.

[25] Shi-Ju Ran. »Encoding of matrix product states into quantum circuits of one- and two-qubit gates«. In: *Physical Review A* 101.3 (Mar. 2020). ISSN: 2469-9934. DOI: 10.1103/physreva.101.032310. URL: http://dx.doi.org/10.1103/PhysRevA.101.032310.

[26] Benyamin Ghojogh et al. »Sampling Algorithms, from Survey Sampling to Monte Carlo Methods: Tutorial and Literature Review«. In: *arXiv preprint arXiv:2011.00901* (2020). URL: https://arxiv.org/abs/2011.00901.

[27] Sarah Lee. »Rejection Sampling: A Deep Dive«. In: (2025). URL: https://www.numberanalytics.com/blog/rejection-sampling-deep-dive.

[28] Dani Gamerman and Hedibert F. Lopes. »A simple introduction to Markov Chain Monte–Carlo sampling«. In: *PLoS Computational Biology* (2016). URL: https://pmc.ncbi.nlm.nih.gov/articles/PMC5862921/.

[29] He-Liang Huang et al. »Superconducting quantum computing: a review«. In: *Science China Information Sciences* 63.8 (July 2020). ISSN: 1869-1919. DOI: 10.1007/s11432-020-2881-9. URL: http://dx.doi.org/10.1007/s11432-020-2881-9.

[30] Francesco Bernardini, Abhijit Chakraborty and Carlos Ordóñez. *Quantum computing with trapped ions: a beginner's guide*. 2023. arXiv: 2303.16358 [quant-ph]. URL: https://arxiv.org/abs/2303.16358.

[31] Marin Ivezic. *IonQ's 2025 Roadmap: Toward a Cryptographically Relevant Quantum Computer by 2028*. 2025. URL: https://postquantum.com/industry-news/ionqroadmap-crqc/.